Neurobiology of Stress 15 (2021) 100403

Contents lists available at ScienceDirect

Neurobiology of Stress

journal homepage: www.elsevier.com/locate/ynstr

The habenula clock influences response to a stressor

Adriana Basnakova [a,b], Ruey-Kuang Cheng [c], Joanne Shu Ming Chia [c], Giuseppe D'Agostino [c], Suryadi [d], Germaine Jia Hui Tan [c], Sarah R. Langley [c], Suresh Jesuthasan [b,c,*]

[a] School of Biological Sciences, University of Manchester, UK
[b] Institute of Molecular and Cell Biology, Singapore
[c] Lee Kong Chian School of Medicine, Nanyang Technological University, 59 Nanyang Drive, 636921, Singapore
[d] School of Physical and Mathematical Sciences, Nanyang Technological University, Singapore

ARTICLE INFO

Keywords:
Anxiety
Circadian clock
Habenula
Spontaneous activity
Predictive coding

ABSTRACT

The response of an animal to a sensory stimulus depends on the nature of the stimulus and on expectations, which are mediated by spontaneous activity. Here, we ask how circadian variation in the expectation of danger, and thus the response to a potential threat, is controlled. We focus on the habenula, a mediator of threat response that functions by regulating neuromodulator release, and use zebrafish as the experimental system. Single cell transcriptomics indicates that multiple clock genes are expressed throughout the habenula, while quantitative in situ hybridization confirms that the clock oscillates. Two-photon calcium imaging indicates a circadian change in spontaneous activity of habenula neurons. To assess the role of this clock, a truncated *clocka* gene was specifically expressed in the habenula. This partially inhibited the clock, as shown by changes in *per3* expression as well as altered day-night variation in dopamine, serotonin and acetylcholine levels. Behaviourally, anxiety-like responses evoked by an alarm pheromone were reduced. Circadian effects of the pheromone were disrupted, such that responses in the day resembled those at night. Behaviours that are regulated by the pineal clock and not triggered by stressors were unaffected. We suggest that the habenula clock regulates the expectation of danger, thus providing one mechanism for circadian change in the response to a stressor.

1. Introduction

Expectations play a major role in determining the response of a person or animal to a sensory stimulus or situation. In this framework, known as predictive coding or active inference, the brain is not a passive recipient of stimuli, but actively generates expectations that are updated by experience (Barrett, 2017; Friston, 2018). Thus, encountering a cue such as the smell or sound of a predator increases the expectation of danger, turning a normally innocuous stimulus into a threat. Abnormal expectations, or predictions, have been proposed to underlie stress-related conditions such as depression (Smith et al., 2021) and post-traumatic stress disorder (Linson and Friston, 2019; Wilkinson et al., 2017). Predictions are mediated in part by spontaneous activity in the brain (Berkes et al., 2011; Koren and Denève, 2017; Pezzulo et al., 2021), while updating of expectations is enabled by the release of neuromodulators. Dopamine and serotonin contribute to the comparison of current input with pre-existing expectations. When outcomes surpass predictions, dopamine release by neurons in the midbrain increases; when there is disappointment, dopamine release is inhibited (Schultz, 1998). Serotonin release by the raphe provides an indication of the magnitude of the prediction error (Matias et al., 2017). Acetylcholine appears to have a role in setting the precision of predictions (Moran et al., 2013). Behaviour and emotional states can thus be understood to be the result of genetically encoded programs that are continuously modified by predictions, enabling the animal to respond optimally to perceived reality.

The habenula, which contains several subdomains, has emerged in recent years as an important regulator of neuromodulators involved in predictive coding. The medial habenula in zebrafish (Hong et al., 2013), like that of mouse (Ren et al., 2011), includes cholinergic neurons. Disruption of specific subdomains of the medial habenula leads to anxiety-like behaviour that is experience dependent (Agetsuma et al., 2010; Lee et al., 2010). The lateral habenula regulates midbrain dopaminergic and serotonergic neurons, and phasic activity occurs here when there is an unexpected punishment or absence of reward (Matsumoto and Hikosaka, 2009). As an animal learns the actions that

* Corresponding author. Lee Kong Chian School of Medicine, Nanyang Technological University, 59 Nanyang Drive, 636921, Singapore.
E-mail address: sureshj@ntu.edu.sg (S. Jesuthasan).

https://doi.org/10.1016/j.ynstr.2021.100403
Received 8 July 2021; Received in revised form 17 September 2021; Accepted 19 September 2021
Available online 23 September 2021

prevent punishment, this activity lessens (Amo et al., 2014). In addition to activity that is evoked by sensory stimuli or perceptions of reward, the habenula displays spontaneous activity (Jetti et al., 2014; Kim and Chang, 2005). Excessive levels of burst firing, which can be interpreted as constant negative prediction, has been detected in the lateral habenula of animals with depressive behavior (Andalman et al., 2019; Yang et al., 2018). To understand how mood and behaviour are shaped, it is thus important to not only understand how the habenula responds to reward and sensory input, but to also investigate how spontaneous activity is regulated.

One factor that affects the level of spontaneous activity in neurons is the molecular clock. The molecular clock in most organisms consists of a transcriptional-translational feedback loop with a period of ~24 h (Takahashi, 2017). Core components of the clock in animals include heterodimers of Clock and Arntl (Bmal), which enter the nucleus in the daytime. Here, they drive transcription of *period* (*per*) and *cryptochrome* (*cry*) genes, which then inhibit the Clock-Arntl heterodimer. Clock and Arntl also control transcription of channels that affect resting membrane potential in neurons, driving this close to threshold and thus increasing spontaneous firing rate in the daytime (Harvey et al., 2020). Components of the clock machinery are found in nearly all cells, including those of the habenula (Baño-Otálora and Piggins, 2017; Mendoza, 2017), and the habenula molecular clock continues cycling for multiple days even in the absence of the main pacemaker of the brain, the suprachiasmatic nucleus (Guilding et al., 2010; Salaberry et al., 2019). Spontaneous firing in the habenula of rat (Zhao and Rusak, 2005) and mouse (Guilding et al., 2010; Sakhi et al., 2014a, 2014b) varies across a circadian cycle, in both the lateral and medial habenula. The significance of the habenula clock is unclear, however. Given the role of habenula activity in predictive coding, we hypothesize that the clock causes a circadian change in behaviours that are modified by recent experience. To test this, we use the zebrafish as the experimental system. We examine anxiety-like behaviour, which is increased by expectation of danger.

2. Materials and methods

2.1. Single cell data reanalysis

Count tables were downloaded from Gene Expression Omnibus, accession number GSE105115. All processing downstream was done using R/BioConductor (R 4.0.2/Bioconductor 3.12) packages designed to handle single cell data using the SingleCellExperiment class (v. 1.12.0) (Amezquita et al., 2020). A detailed explanation with code and figures is provided as a GitHub repository at https://github.com/langleylab/habenula_reanalysis. Briefly, gene-level count tables from the SmartSeq2 experiment were merged retaining the information on the plate of origin. Genes that were not detected in any barcode were removed. Barcodes were discarded according to the following criteria: low expression, low number of genes detected, high percentage of *malat1* expression, high percentage of mitochondrial transcripts expression and high percentage of ribosomal transcript expression. Thresholds for every criteria were set as 3 Mean Absolute Deviations (MADs), with the exception of mitochondrial % which was set at 4 MADs. Outlier calculations were done separately in each plate using the *isOutlier* (using the *batch* argument) and *perCellQCMetrics* functions from the *scater* package (v. 1.18.6) (McCarthy et al., 2017). These filters yielded 17673 genes and 1140 barcodes for downstream analyses. Barcodes were then clustered using the *quickCluster* function from the *scran* package (v. 1.18.5 (Lun et al., 2016)), blocking for the plate of origin. Per-cell size factors were then determined by deconvolution using *scran*, and they were used to perform multi-batch normalization (batching by plate) using the *multiBatchNorm* function from the *batchelor* package (v. 1.6.2 (Haghverdi et al., 2018)). Highly variable genes were estimated on the multi-batch normalized data blocking by plate using the *modelGeneVar* function from the *scran* package, which estimates the mean-variance trend and decomposes variance for each gene in technical and biological components according to the deviation from the trend. Variances were combined across plates using the *combineVar* function from *scran*, and the 2000 genes with the highest biological variance were selected using the *getTopHVGs* function from *scran*. These were used as an input to perform dimensionality reduction via Principal Component Analysis as implemented in the *BiocSingular* package (v. 1.4.0, (Lun, 2020a)).

The first 50 principal components were then used as an input to perform batch (plate) effect correction via the *fastMNN* function from *batchelor*, which determines a correction vector in PCA space using mutual nearest neighbour pairs to estimate the amount and direction of necessary correction. The dimensionality of the corrected space, i.e. the number of most relevant dimensions for subsequent steps, was determined using the *maxLikGlobalDimEst* function from the *intrinsicDimension* package (v. 1.2.0 (Johnsson et al., 2014)). The value for the *k* parameter for this function (k = 30) was determined as the rounded square root of the number of cells, and the estimation yielded 13 dimensions. Subsequently, the first 13 dimensions of the corrected space were used to run the uniform manifold approximation and projection (UMAP) algorithm for data visualization (McInnes et al., 2018), and to construct a Shared Nearest Neighbour (SNN) graphs for clustering. Several SNN graphs were constructed at different resolutions, i.e. 10, 15, 30, 40 and 50 neighbours were considered for the graph construction; all edges were weighted by the Jaccard similarity between the neighbours of each node. SNN graph construction was performed using the *buildSNNGraph* function from *scran*. Then, the Louvain community detection algorithm (as implemented in the *igraph* package (v. 1.2.6 (Csardi and Nepusz, 2006)) was used to identify clusters. Relationships between different clustering results (obtained by using different neighbours in the SNN graph construction) were inspected using a clustering tree drawn using *clustree* (v. 0.4.3 (Zappia and Oshlack, 2018)). Clusterings with 10 and 15 neighbours were further explored, as they yielded numbers of clusters similar to the ones in the original publication. For both 10 and 15 neighbours, cluster separation was evaluated using three methods: approximate silhouette width, neighborhood purity and pairwise modularity, as implemented in the *bluster* package (v. 1.0.0 (Lun, 2020b)) in the *approxSilhouette*, *neighborPurity* and *pairwiseModularity* functions. The 15 neighbour clustering showed slightly better separation so it was considered for downstream analyses. In order to reconstruct the original cell type identities as identified by the authors, the *AUCell* package (v. 1.12.0, (Aibar et al., 2017) was used in conjunction with the cluster marker genes as published by the authors, although these marker genes were identified in the 10X dataset. Raw counts were ranked in each cell and the AUC for each marker set was calculated; each cell was assigned the identity yielding the highest AUC value using the 30% top ranking genes. AUCell is agnostic to the transcriptional space and to other intrinsic properties of the dataset, which will be influenced by differences in filtering and processing steps. Therefore the performance of AUCell was evaluated in this dataset calculating the approximate silhouette width of the cell type assignment, and it was compared to our clustering results by calculating pairwise Jaccard indices. Most identities (Hb1, Hb2, Hb5, Hb6, Hb9, Hb1, Hb14, Hb15 and olfactory neurons) are reasonably well separated, but only 4 (olfactory, Hb06, Hb03, and Hb08), are reproduced in our clustering with a Jaccard index above 0.5 with any single cluster. This is in line with what the authors of the original paper state regarding the poor performance of SmartSeq2 in terms of cell type recovery, and is also to be expected when using cell type markers identified in the 10X dataset.

For the 10X datasets (larval) no filtering was performed as the distribution of QC metrics was well within standard ranges, suggesting data were already filtered. Normalization, HVG estimation and dimensionality reduction were performed in the same way as described above, with the exception that there was no batch effect to account for and correct. An additional doublet detection step was included using the *scDblFinder* package (v. 1.4.0, (Germain et al., 2020), which flagged 172

barcodes as doublets and 4193 as singlets. Doublets were not removed at this stage of the analysis. The intrinsic dimension estimation (k = 66) yielded 12 dimensions to perform SNN graph clustering, which was performed using 5, 10, 15, 20, and 30 neighbours. In parallel, 36 dimensions were also considered as done by the authors of the original publication. For the 12-dimensional space, 5 and 10 neighbours were considered as they yielded numbers of clusters similar to those reported in the publication; for the 36-dimensional space, 10 and 15 neighbours were considered. However, in both 12 and 36 dimensions a cluster was entirely made up of doublets, so doublets were removed and the whole process (normalization, HVG selection and dimensionality reduction) was repeated. Cluster separation metrics (approximate Silhouette and modularity) favoured clustering with 10 neighbours (12 dimension) and 15 neighbours (36 dimensions). To reproduce the original clustering results the AUCell package was used, and Jaccard indices were used to match clusters to labels. In order to improve the label assignment, cells whose top AUC label showed less than a 20% difference from the second best label were classified as "ambiguous". Ambiguous labels were then reassigned using the closest centroid in the approximate silhouette width calculation, thus making the labels conform more to the transcriptional space. Improvements in the reassignment of these labels were measured by comparing silhouette widths and the distribution maximum Jaccard indices for every cluster-AUC label pair before and after reassignment. Both metrics showed an improvement in both silhouette width and median best Jaccard index upon reassignment.

Adult zebrafish data was processed in the same above, accounting for batch effects (2 different captures). SNN graph construction with 4 neighbours in 16 dimensions was chosen following the same pipeline and reasoning used in the larval dataset. AUCell was used to determine identities using the markers provided by the authors of the original publication, and the reassignment procedure described above was used to correct ambiguous labels.

2.2. Transgenic lines

TgBAC(gng8:GAL4)^{c426} (Hong et al., 2013) or*T*^{s1011t} (Scott and Baier, 2009) was used to drive expression in the habenula. Calcium imaging was performed using *Tg(elavl3:GCaMP6f)*^{a12200} and *Tg(UAS:GCaMP6s)*^{sq205}. *Tg(UAS:EGFP-2A-Δclocka-5×MYC)*^{sq215}, abbreviated here as *Tg(UAS:EGFP-Δclocka)* was generated by injection of *pT2-UAS:EGFP-2A-Δclocka-5xMYC* using Tol2 mediated transgenesis. All experiments were carried out under guidelines approved by the IACUC of Biopolis (181408) and NTU (A19014). The minimal number of animals was used. Fish were maintained in a Techniplast system, with a light/-dark cycle of 14/10 h and a water temperature of 28 °C.

2.3. Two-photon imaging

2.3.1. Extended imaging

Based on the methods described by (Leung et al., 2019), non-anesthetized and non-paralyzed larvae were mounted in 2% low melting agarose (LMA), in a glass-bottom dish (Matek). The dish was filled with E3 medium supplemented with 1% Hepes and bubbled continuously with carboxygen (95% oxygen). Imaging was performed with a Nikon A1R MP system, attached to an upright FN1 microscope using a 25 × 1.0 NA water dipping objective. Resonant scanning was performed with 2× averaging, and 20 focal planes were collected, spaced 5 μm apart. Signal was detected with a GaAsP detector. A piezo drive (Mad City Labs) was used for fast focusing during imaging. 21 stacks were collected, at an interval of 1 s, followed by a delay of 1 h. The maximum imaging duration was 29 h. After imaging, larvae were checked for blood flow. They were then released from the agarose. Only data from fish with normal blood flow and active swimming upon release were used for analysis.

To obtain a measure of calcium levels in the whole habenula, fluorescence intensities were summed at each time point using Fiji. The intensity at each hour was averaged and z-scores were plotted as a function of *zeitgeber* time. Statistical analysis was performed with Prism, by nonlinear regression to a sinewave.

2.3.2. Short duration imaging

6-day-old *Tg(elavl3:H2B-GCaMP6s)* or *Et(-1.5hsp70l:Gal4-VP16)*^{s1011t}*, Tg(UAS:GCaMP6f)* larvae were immobilized with mivacurium, mounted in 2% low melting temperature agarose and imaged with the two-photon system described above, using resonant scanning at a single plan. Frame size was 512 × 256 pixels and 2× averaging was used, leading to a frame rate of 14.5 Hz. Segmentation of cells expressing cytoplasmic GCaMP6f was performed manually in Fiji, while segmentation of cells expressing nuclear GCaMP6s was performed automatically with Suite2p (Stringer and Pachitariu, 2019). Z-scores were obtained for each cell in a recording, and cells were clustered using K-means clustering in Python. The classification was performed using maximum likelihood and leave-one-out cross-validation. Specifically, at each iteration we removed one dataset from the group and constructed empirical cluster distributions for both categories (ZT3 and ZT15) from the remaining datasets. The removed dataset was then assigned to the category whose empirical distribution maximized its likelihood. This process was repeated independently until all datasets were classified.

2.4. Immunohistochemistry and imaging of EGFP-ΔCLK

The *Tg(gng8:GAL4,UAS:EGFP-Δclocka)* larvae at the age of 7 dpf were fixed in 4% PFA at 4 °C for ~22 h. For immunostaining of extracted brains, skin covering the brain was manually removed and exposed brains were washed 3 times in PBST. Antigen retrieval was performed by incubating the fish in 150 mM Tris-HCl (pH 9.0) for 5 min at room temperature in order to equilibrate, and by subsequent heating of the samples at 70 °C for 15 min. Following several washes and a blocking step, samples were incubated in the rabbit anti-GFP primary antibody (Torrey Pines Biolabs Inc., #TP401), diluted 1:500, and the mouse anti-Myc antibody (9E10; Santa Cruz Biotechnology), diluted 1:100, at 4 °C for a few days. The secondary antibodies used were Alexa Fluor 488 goat anti-rabbit (ThermoFisher and Abcam), diluted 1:1000, and Alexa Fluor 647 goat anti-mouse (ThermoFisher), diluted 1:500. The immunostained brains were mounted in 2% LMA in PBS and imaged using a Zeiss LSM800 confocal microscope equipped with 40X 0.7 NA water immersion objective.

2.5. Screening and selection of Tg(gng8:GAL4,UAS:EGFP-Δclocka) fish

All of the *Tg(gng8:GAL4,UAS:EGFP-Δclocka)* fish used in the following experiments were first screened for GFP fluorescence at 3 dpf using an Olympus MVX10 or Zeiss V16 stereo fluorescence microscope. Since the expression of EGFP-ΔCLK in the habenula was mosaic, only individuals with expression in the majority of habenula cells were selected and used for further experiments as ΔCLK-positive fish. To maximize expression, fish were generated by in-crossing. A consequence of this, however, is that fish with zero expression were rare. Thus, in addition to individuals with zero expression, larvae exhibiting a minimal number of randomly labelled cells (less than 15 cells per fish) were used as the control siblings (Fig. S1). Despite this, the size of the control group was smaller than the ΔCLK group.

Following the behavioural experiments, larvae were immobilized in tricaine methanesulfonate (MS-222; final concentration of 0.01 mg/mL; Sigma), mounted in 2% LMA in E3 medium and the habenula-specific expression of EGFP was assessed using a Zeiss LSM800 confocal microscope and 40X water dipping objective.

2.6. Quantification of DA and 5-HT levels

Three-month old female ΔCLK fish and their control siblings were immobilized using iced water and euthanized by decapitation at ZT3 and

ZT15. Whole brains, excluding the olfactory bulb, were extracted in the ice-cold Ringer's solution (116 mM NaCl, 2.9 mM KCl, 1.8 mM $CaCl_2$, 5.0 mM HEPES, pH 7.2), snap-frozen in liquid nitrogen and stored in −80 °C until further analysis. Supernatant was collected as described previously (Chatterjee and Gerlai, 2009). Quantification of dopamine (DA) and serotonin (5-HT) was carried out by LC/MS using the following analytical standards: dopamine hydrochloride (D2960000: Sigma-Aldrich), dopamine-1,1,2,2-$d_4$hydrochloride (73483: Sigma-Aldrich) and serotonin (14927: Sigma-Aldrich). Three biological replicates (i.e. measurements of different samples) were performed.

2.7. Behaviour assays

2.7.1. Acoustic startle following exposure to Schreckstoff

Thirteen to sixteen day-old ΔCLK larvae and their non-expressing siblings were placed in two transparent plastic tanks with dimensions of 80 × 54 x 33 (L x W x H in mm) and their locomotor activity was recorded from above at 10 fps using a camera (acA2040-90μm USB 3.0; Basler). Each of the two tanks was filled with 20 mL of facility water and held 6–8 fish. The water level in each tank was 5 mm in height to minimize vertical movement. The alarm substance was freshly prepared from adult zebrafish each week (Mathuru et al., 2012), and was tested for effectiveness on adults before use on larvae. An Arduino Grove Vibration Motor was positioned in between the two plastic tanks, on the stage holding the tanks, to provide the stimulus. The vibration was 1 s in duration and was presented 3 times, at 1 min intervals, starting 5 min before and after the delivery of the *Schreckstoff*. A startle response was defined as a change in body orientation of more than 90° within 5 s in response to each vibration tone. The response (yes or no for each fish) was averaged across 3 tones for each group to obtain a response percentage before and after the delivery of the *Schreckstoff*. Both the vibration tones and the delivery of *Schreckstoff* were controlled by an Arduino board synched with the video-recording Python codes. Experiments were performed on 3 separate batches of larvae. A different batch of freshly prepared skin extract was used for each experiment; the extract was verified for effectiveness by testing on adult fish. Only extract that evoked freezing was used.

2.7.2. Locomotor activity and sleep analysis

The *Tg(gng8:GAL4,UAS:EGFP-Δclocka)* larvae were raised under standard conditions. Each experimental run involved animals from the same batch, originating from one pair of parents. The larvae were screened and selected as described in the previous section. At the age of 6 dpf the larvae were placed individually in a 24-well plate filled with 1.5 mL of tank water per well. The plate was then transferred into an incubator equipped with an IR camera (acA2040-90μm USB 3.0: Basler), a white LED box and four IR LED bars (LBS2-00-080-3-IR850-24V, 850 nm: TMS Lite). The camera and the LEDs were connected to a PC via a microcontroller board (Arduino UNO SMD). At the onset of recording (ZT6 – 9), fish were kept under ambient light, which was switched off at ZT14 and was kept off during the next day for the monitoring of activity under DD. A customized script written in Python 2.7 (see https://github.com/rkcheng/SleepRecording-and-CircadianStartleResponse), incorporating functions from the OpenCV library was used to control the Arduino microcontroller and simultaneously video-track fish locomotor activity. The video was captured using 576 × 864-pixel resolution at 10 frames per second and the background subtraction method was implemented to extract the 'x' and 'y' coordinates of each fish online. The position data was then converted to total distance (mm) travelled by each fish per 1 min time. A sleep bout (or a rest bout in the subjective day or light phase) is defined as a continuous period of inactivity lasting 1 min or longer. The threshold of detecting any inactive minute is set at no more than 1 s active in a given minute. The data conversion, further analysis and plotting were carried out using custom-written Excel macros, Python 2.7 and Estimation Statistics (Ho et al., 2019).

2.7.3. Arousal threshold

Six days-old ΔCLK larvae and their control siblings were randomly placed in a 24-well plate and their locomotor activity was video-tracked as described in the previous section. In order to assess the arousal during sleep, vibration stimuli were applied through a speaker controlled, via an Arduino microcontroller board, by a modified version of the activity-tracking code in Python 2.7. Starting at ZT17, eighteen stimuli of nine different intensities, where 50% of computer audio output represented the highest intensity, were delivered for 200 ms (starting from 0%) in 12–16% increments every minute, first in a descending and then ascending order. The time interval between stimuli was determined based on previous findings that suggest a 30-s inter-stimulus gap is sufficient to avoid behavioural habituation (Burgess and Granato, 2007). The protocol was repeated at the commencement of every hour until ZT22, while the onset by ascending or descending order was altered each time. In total, 12 replicates (i.e. technical replicates) of each stimulus intensity were generated. A fish was scored as responding if it moved more than 7 pixels (~4 mm) following the stimulus delivery and the average percentage of responding fish was calculated for each of the stimulus intensities (Woods et al., 2014). The observed values were corrected for variations in the baseline locomotor activity, by first calculating the background probability of locomotion as a percentage of larvae which moved more than 7 pixels 5 s before the application of each stimulus. The average of 108 measures of the background probability of locomotion was then used to calculate the corrected probability of response at each of the stimulus intensities, implementing the following equation: corrected probability of response = observed value x [(observed value - background offset)/(max observed value - background offset)].

2.7.4. Novel tank assay

All experiments were conducted between ZT2 and ZT4 on 3-5 month-old adult zebrafish, as described elsewhere (Haghani et al., 2019). Fish were recorded in pairs in a darkened room with a black background, where tanks were illuminated from the top with a natural light LED bar. Novel tanks were made of glass measuring 20 cm (L) by 5 cm (W) by 12 cm (H) with opaque sides (to prevent fish from viewing each other), placed side by side. Fresh water from the facility was added to tanks up to the 10 mL mark to make a total volume of 1 L. The setup was placed within a curtained area to obscure the experimenter.

Prior to exposure to the novel tank, fish were handled carefully to ensure that handling stress was minimized. Fish were gently netted in pairs from their home tanks in the facility to smaller crossing tanks, where they were brought into the room with the behavioural setup. Then, fish were netted into 100 mL beakers with ~30 mL of fish facility water and quickly poured into the novel tank. The recording was started within 30 s of fish being in the recording tanks. For exposure to *Schreckstoff,* fish were placed in 100 mL beakers containing 200 μL of heated skin extract (Chia et al., 2019) in 50 mL fish facility water for 2 min. Fish were netted into another beaker containing fresh facility water before being poured into the novel tank. Videos were acquired at 10 frames per second for 600 s (10 min) using a Basler Ace camera (acA1300–200 μm; 1280 × 1024). The position (x-y coordinates) of the fish were tracked, and speed was binned by mm/s into a probability density curve.

For acute exposure to *Schreckstoff*, fish were first habituated in the glass tanks for 5–7 min. Then, fish were recorded in the tanks for 5 min before 1 mL of 1:4 dilution of heated skin extract was pipetted into the tanks. The recording continued for 5 min after *Schreckstoff* delivery for the alarm response to be observed. Two fish were tested at one time, each in a separate tank, with one tank containing ΔCLK fish and the other a non-expressing sibling. The tank used for a particular genotype was switched at every trial. Characteristic alarm responses were quantified, such as time spent in the bottom third of the tank, number of darting episodes (fish speed >5 SD above average swim speed for the first 5 min), and number of freezing episodes (movement of <5.5 mm

per second). Tracking was automated to prevent observer bias. Sample size was based on previous experiments (Chia et al., 2019).

2.7.5. Light/dark choice assay

All experiments were performed between ZT2 and ZT9 in a behavioural arena within blackout curtains as described previously (Cheng et al., 2016). Four transparent plastic tanks (dimensions: 43 mm W × 60 mm L × 30 mm H) filled with 30 mL fresh tank water served as assay chambers. Opaque cardboard sheets were placed between the 4 tanks. Tanks were placed on an Apple iPad screen and videos (9 fps) were recorded on a USB3.0 Basler camera (Model# acA2040-90umNIR 1440 × 1080 pixels) with a long-pass filter (MIDOPT, LP830 830 nm) placed above. Two IR light bars (850 nm peak from TMS-lite) positioned next to the 4 tanks served as an IR light source. The light/dark compartments were created by white and black rectangles (with 50% transparency level for the black) on a Microsoft PowerPoint slide displayed on the iPad Air at highest brightness level. Sample size was based on previous experiments (Cheng et al., 2016).

Larvae were exposed either to *Schreckstoff* or to control water (embryo medium) in a treatment tank of the same dimensions with the same volume of tank water for 10 min. Larvae were then gently pipetted from the treatment tank into two wash-out tanks sequentially before being placed into the dark/light test chamber. Real-time tracking of the fish was achieved by custom-written Python codes using the OpenCV library and recorded as coordinates of the centroid of the fish across time. Larval behaviour was recorded for 10 min. Offline analysis was performed using custom-written Excel macros to determine the position of the animals, the number of entries into each compartment, the percentage of total time spent in each compartment, etc. A few fish (N = 2 in both the Control group and Gng8/ΔCLK group) were excluded from the analysis because they were entirely immobile or because of tracking errors.

2.8. In situ hybridization

Hybridisation chain reaction with split initiator probes was conducted using the HCR v3.0 protocol for whole-mount zebrafish embryos and larvae from Molecular Instruments. Probe hybridization buffer, amplification buffer, probe wash buffer, probe sets and HCR amplifiers were obtained from Molecular Instruments.

Tg(gng8:GAL4, UAS:EGFP-Δclocka) larvae were maintained at 28 °C under the standard 14-10h light-dark (LD) cycle. For characterization of clock genes under DD, nacre and *Tg(gng8:GAL4, UAS:EGFP-Δclocka)* larvae were maintained under standard LD conditions transferred to a dark room at ZT14 the day before fixation.

All *Tg(gng8:GAL4, UAS:EGFP-Δclocka)* larvae were screened for mosaic expression of EGFP-ΔCLK at 5 dpf and EGFP-ΔCLK positive larvae were separated from non-expressing siblings. All larvae were fixed at ZT3, ZT7, ZT11, ZT15, ZT19 and ZT23h with 4% paraformaldehyde (PFA) in phosphate buffered saline (PBS) at 4°C in a 1.5 mL eppendorf tube (1 tube per time-point) and incubated at 4°C overnight. Fixations for DD larvae were performed under dim light. For dehydration and permeabilization, larvae were washed 4 × 10 min and 1 × 50 min with 1 mL of 100% methanol (MeOH) at room temperature, and subsequently stored in −20°C for several days. For rehydration, larvae were washed 1 × 5 min with 1 mL of 75% MeOH (in PBST), followed by 50%, and 25% MeOH (in PBST), and subsequently 5 × 5 min washes with 100% PBST. Larvae were then treated with 1 mL of 30 μg/mL proteinase K for 45 min at room temperature and washed twice with 1 mL of PBST without incubation. Postfixation of larvae was conducted by adding 1 mL of 4% PFA for 20 min at room temperature. The larvae were then washed 1 × 1 h and 4 × 5 min with 1 mL of PBST. For prehybridization, 4 larvae from each sample were transferred to a 1.5 mL eppendorf tube and 500 μL of probe hybridization buffer was added and incubated at 37°C for 30 min. For detection of clock genes, probe hybridisation buffer was aspirated from the samples and probe solution (2 μL each of 1 μM *arntl1b* and *per3* qHCR probe sets or 3 μL of *cry1a* dHCR probe set in 500 μL of probe hybridisation buffer at 37°C) was added and incubated at 37°C for ~22 h. Samples were washed 4 × 15 min with 500 μL of probe wash buffer at 37°C, followed by 2 × 5 min washes with 500 μL of 5X SSCT at room temperature for removal of excess probes. 5X SSCT was aspirated from the samples and 500 μL of amplification buffer was added and incubated for 30 min at room temperature. For amplification of signal, amplification buffer was aspirated from the samples and hairpin solution (10 μL each of snap-cooled HCR amplifier hairpins h1 and h2 for all 4 probe sets in 500 μL of amplification buffer at room temperature) was added and incubated in a dark box at room temperature for ~22 h **(qHCR) or 1 hour (dHCR)**. Hairpin solution was then removed by 2 × 5 min and 2 × 30 min washes and another 1 × 5 min wash with 500 μL of 5X SSCT at room temperature. Samples were lastly stored at 4°C in a dark box before microscopy.

2.8.1. qHCR imaging

4 larvae from each sample were mounted in 2% LMA in PBS in dorsal view and imaged using a Zeiss LSM800 upright confocal microscope with 40× water dipping objective at 0.5× zoom. The acquisition settings were identical in all experiments. Z-stacks were collected at 512 × 512 resolution, giving a x-y pixel size of 0.62 μm, and a z-step of 0.73 μm. Sample size was based on (Trivedi et al., 2018).

2.8.2. Image analysis

To quantify gene expression in the entire habenula across different fish, segmentation of habenula was performed manually using the Segmentation Editor in Fiji (Schindelin et al., 2012). The integrated intensity of *per3* and *arntl1b* was measured using the 3D Objects Counter (Bolte and Cordelières, 2006). The ratio was calculated to compensate for potential tube-tube variation as well as change in intensity with imaging depth. Values were plotted using GraphPad Prism.

To compare the level of *per3* in ΔCLK expressing and non-expressing cells, within-fish analysis was performed on single planes. ΔCLK cells were segmented by thresholding the GFP signal, while the habenula was manually segmented. Masks for control cells were obtained by subtracting the ΔCLK mask from the habenula mask. ROIs were then created, and mean intensity measured, based on methods described by (Choi et al., 2018), i.e. with a mean filter of 3 and background correction. Statistical analysis was performed with estimation statistics (Ho et al., 2019).

2.8.3. dHCR imaging

Following label for *cry1a*, 3 larvae from each of 6 time-points were imaged with confocal microscopy, using an Achroplan 63× water dipping objective and 2048× 4093 image size, giving a x-y pixel size of 0.0495 μm z step was 0.78 μm. Sample size was based on Choi et al., 2018. To analyse the images, the habenula in one plane ~10 μm from the surface was manually segmented. Spots were identified in Fiji using a Laplacian transform with FeatureJ, with the smoothing scale set at 5. The number of spots was counted using FindMaxima, with the prominence >10.0. Identical settings were used for acquisition and analysis of all dHCR images.

3. Results

3.1. Multiple clock genes are expressed in the zebrafish habenula

Using in situ hybridization in brain sections with DIG-labelled probes, a number of clock genes, such as *per1b* and *bmal* (*arntl1a*), have been shown to be expressed in the habenula of adult zebrafish (Weger et al., 2013). To better characterize clock gene expression in this structure, we analysed single cell transcriptomes of the zebrafish habenula (Pandey et al., 2018). A diversity of clock gene components, including *arntl1b*, *arntl2*, *per1a*, *per2*, *per3*, *cry1a*, *cry1ab*, *cry1ba*, *cry1bb*, *clocka*, *clockb* and *nr1d1* were found (Fig. 1). These transcripts were

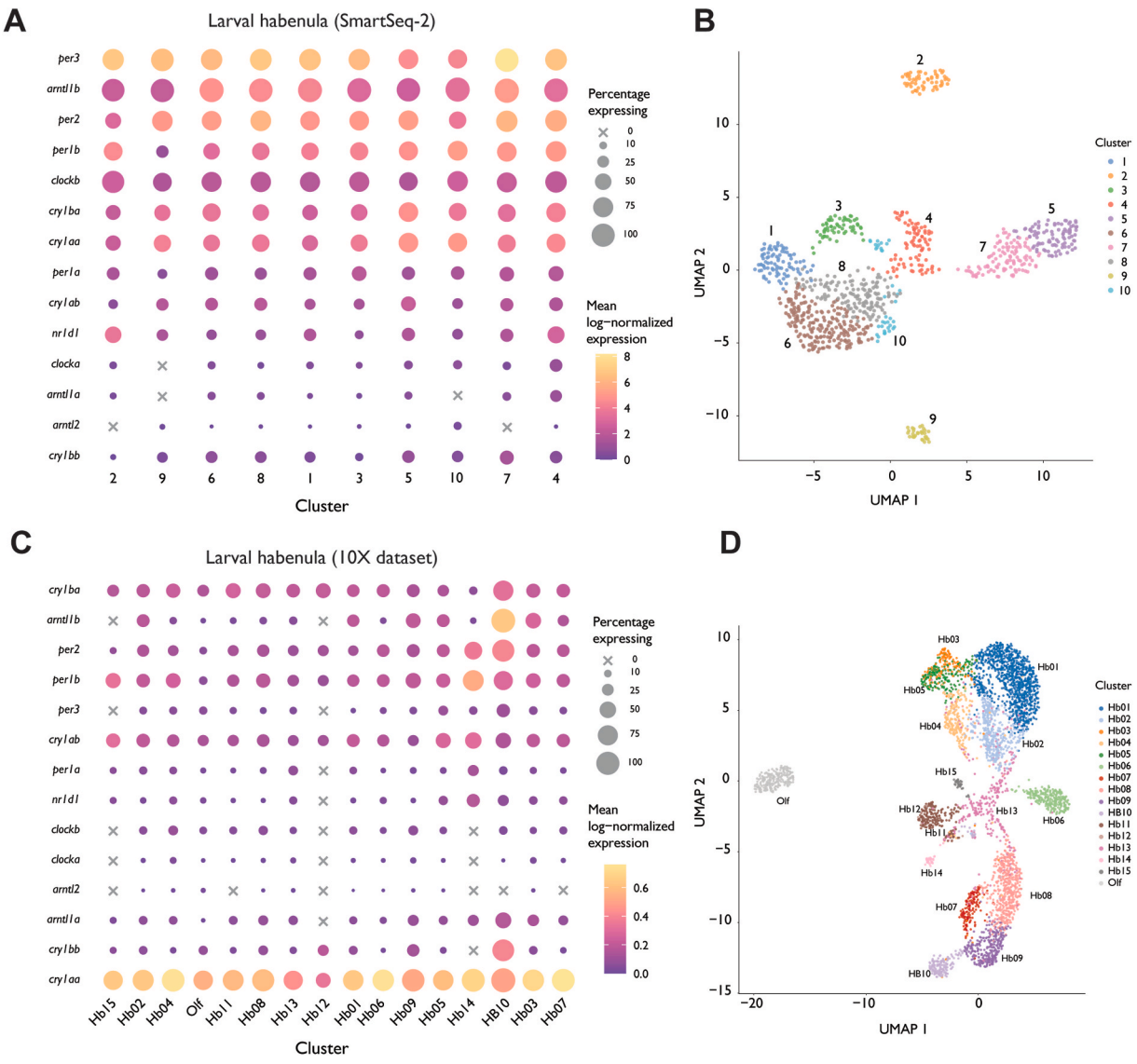

Fig. 1. Clock genes expression in the zebrafish habenula based on single cell RNA sequencing
A) Dot plot showing mean log-normalized expression per cluster and percentage of cells per cluster expressing each gene in the SmartSeq-2 dataset from Pandey et al. **B)** t-SNE representation of clustering results in the SmartSeq-2 dataset. Each point is a cell. **C)** same as A) but in the 10X dataset. **D)** same as C but in the 10X dataset. The cluster assignment for the 10X dataset corresponds to those assigned by Pandey et al., (2018).

isolated from *gng8*-expressing habenula neurons, which are found throughout the habenula (Hong et al., 2013; Pandey et al., 2018). All clusters contained clock genes, suggesting that the molecular clock is broadly distributed.

To examine the temporal dynamics of the clock in larval zebrafish, quantitative in situ hybridization using hybridization chain reaction (HCR) (Choi et al., 2018) was carried out on fish that were fixed at 6 different time points (Fig. 2). With qHCR imaging, *arntl1b* appeared to be expressed at a higher level in the habenula compared to the rest of the brain (Fig. 2A), with a stronger signal at approximately *zeitgeber* time ZT 15; expression at ZT 19 and ZT 23 was detected at the posterior margins. *per3* was detectable broadly in the brain, including the entire habenula, with strongest expression at ZT 23 and ZT 3 (Fig. 2B). Signal intensity obtained with qHCR imaging provides a relative measure of transcript level (Choi et al., 2018), and can vary with sample thickness and between tubes. To minimize error from these potential confounds, we calculated the ratio of *arntl1b/per3* as a means of comparing gene expression between animals. This ratio, which also maximizes sensitivity given the antiphasic expression of the genes, showed a circadian variation with a peak at ZT 11–15 (Fig. 2D). To test whether clock gene cycling requires light, we examined expression in fish grown in constant darkness. The ratio of *arntl1b/per3* expression was maximal at CT 15 and minimal at CT3 (Fig. 2E–G). We used single molecule imaging, with dHCR imaging of *cry1a*, to further test whether the clock is cycling. Again, a circadian change in expression level was detected in the habenula in constant darkness (Fig. 2H and I), with a peak at CT3 and a trough at CT15, similar to what has been reported in other tissues under LD (Cavallari et al., 2011) or DD conditions (Kobayashi et al., 2000). These observations confirm previous findings using clock reporters (Wang et al., 2020; Weger et al., 2013) that the molecular clock is active in the zebrafish habenula.

3.2. *The zebrafish habenula displays circadian variation in intracellular calcium*

The presence of the molecular clock should lead to a number of circadian changes in a cell. One such change is the level of cytoplasmic calcium (Pennartz et al., 2002). To examine intracellular calcium levels

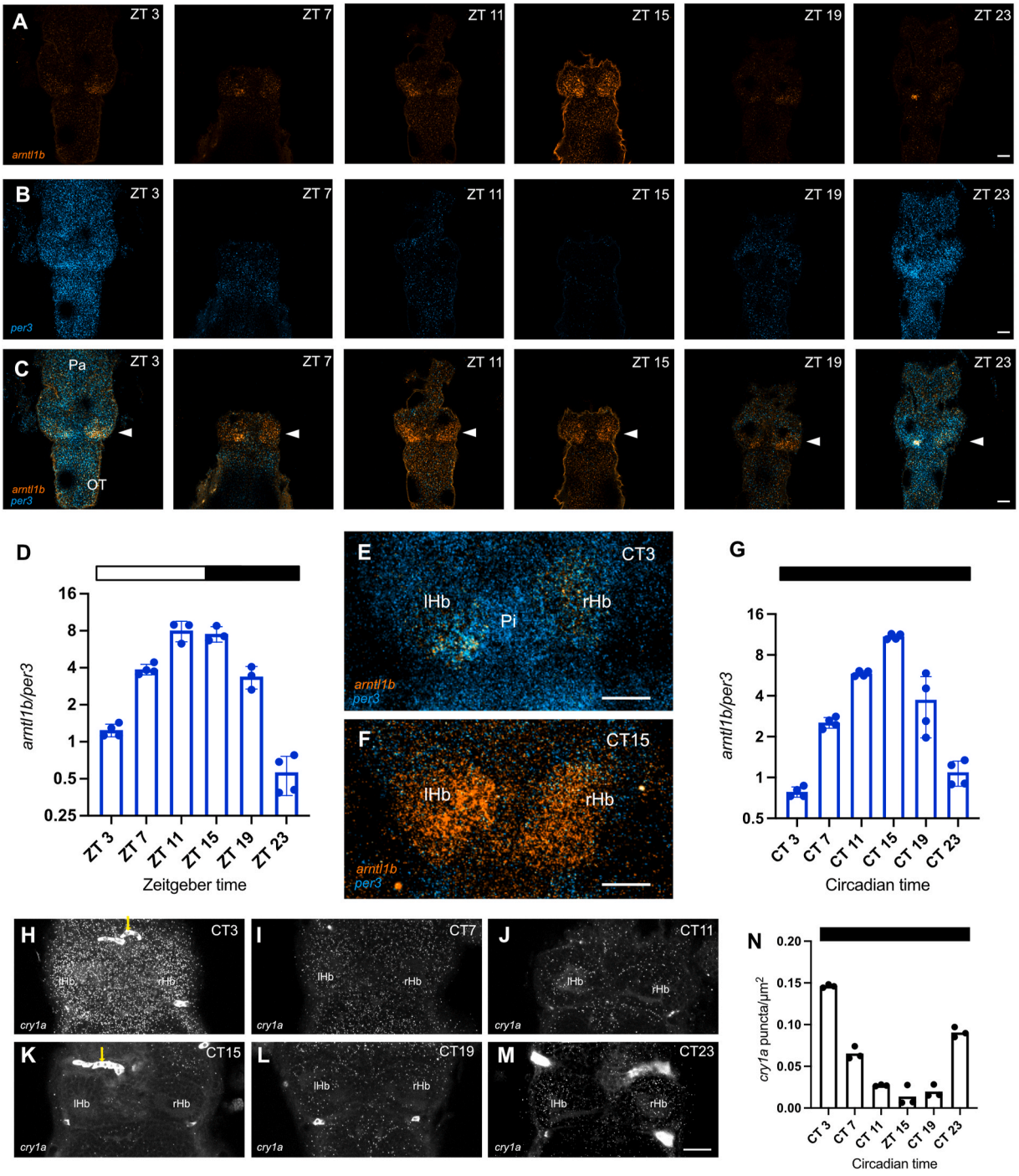

Fig. 2. Dynamics of clock gene expression in the zebrafish habenula. (A–C). Single optical sections of the brain of 6 day old larvae fixed at six different time points, labelled for *arltn1b* (A) and *per3* (A) using hybridization chain reaction. **(C)** Merge of (A) and (B). Arrowheads indicate the habenula. (**D**) Ratio of *arntl1b/per3* in the habenula of fish in a normal LD cycle. (**E-G**) Expression of *per3* and *arntl1b* in the habenula of fish grown under DD conditions. (**H–N**) *cry1a* expression in the habenula of fish grown under DD conditions. Images in E and F are maximum projections of the entire habenula. Images in panels H–M are maximum projections spanning 5 μm. The arrowheads indicate autofluorescent blood cells. A, B, C, E, F, H-M are dorsal views with anterior to the top. The dots in panels D, G and N indicate values for individual fish. The horizontal bars indicate illumination conditions. lHb: left habenula; rHb: right habenula; Pi: pineal; Pa: pallium; OT: optic tectum. Scale bar = 25 μm.

in the zebrafish habenula, two-photon imaging was carried out in fish held in constant darkness. Confocal microscopy was not used to avoid light-induced disruption of the molecular clock by visible light (Tamai et al., 2007). By imaging a series of z-stacks every hour, such that the entire habenula could be captured (Fig. 3A–D), we observed a decrease in fluorescence intensity during the subjective night and an increase in during the subjective day (Fig. 3E; 5 out of 6 fish imaged). The average trace fitted a sine wave (brown line in Fig. 3E) with a period of 20.5 h [95% CI 19.7, 21.5; R^2 = 0.869] and baseline of 0.0 [95% CI -0.17, 0.07]. This finding is consistent with the hypothesis that the habenula contains an active molecular clock that has the potential to drive changes in the intracellular calcium even in the absence of light, a prominent circadian *zeitgeber*.

In the mouse, neurons in both medial (Sakhi et al., 2014a) and lateral

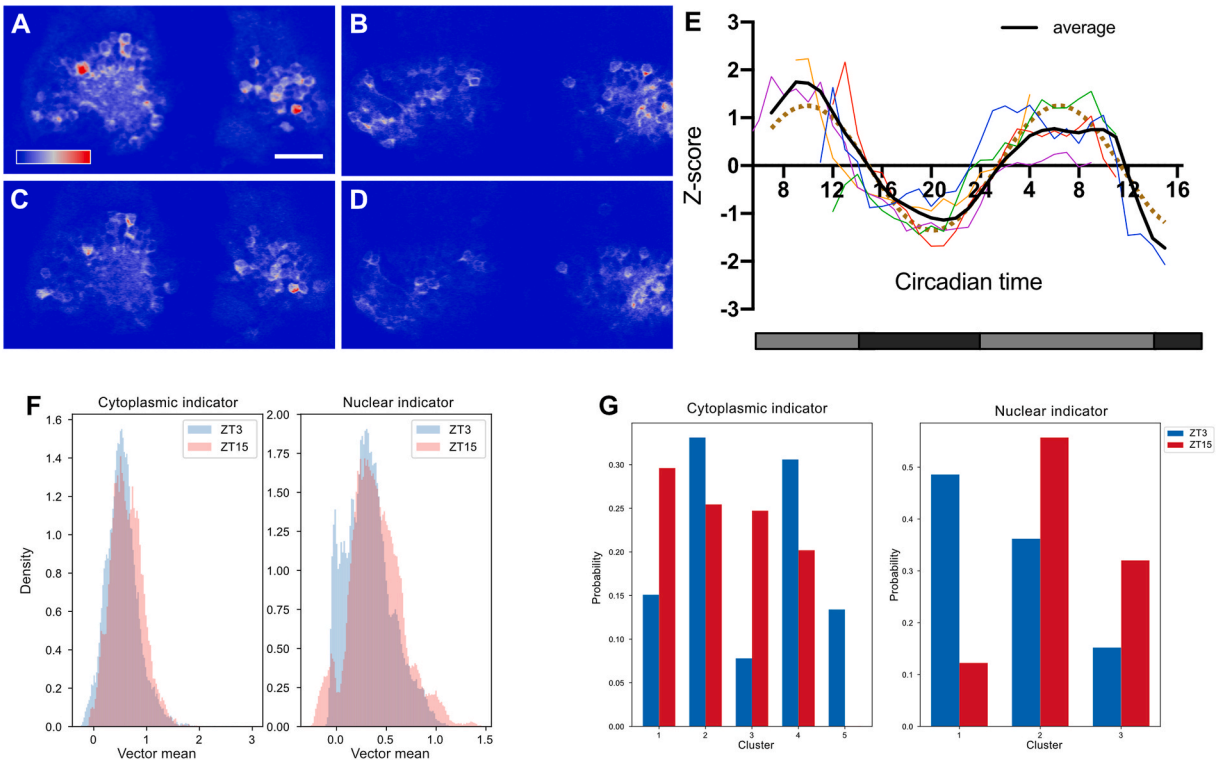

Fig. 3. Circadian variation in cytoplasmic calcium in habenula neurons. (**A-E**) Long duration multiplane recording of the habenula of *Et(GAL4s1011t),Tg(UAS:GCaMP6s)* larvae in constant darkness. (A–D) Examples of imaging data from one fish at two different time points, ZT5 (A, B) and ZT14 (C, D), and two different focal planes, dorsal (A, C) and ventral (B, D). Scale bar = 25 μm, dorsal view with anterior to the top. The wedge shows the look up table (LUT) used to represent pixel intensities, with values ranging from 3 (blue) to 3939 (red). (E) Average level of cytoplasmic calcium in the habenula, as shown by intensity of GCaMP6s. Each coloured trace represents a different fish. The thicker black line is the mean. There is a reduction in intracellular calcium levels during the subjective night and an increase in the subjective day. The dotted brown line is a sine wave that the data was regressed to, with an R^2 of 0.869. (F–G) Difference in relative activity levels of habenula neurons between day (ZT3) and night (ZT15) as measured by both cytoplasmic and nuclear GCaMP6s. (F) Distribution of the mean of vectors containing z-scores of neurons with high variance in their activity. The distributions are different, as determined by Kolmogorov-Smirnov test, with $p < 0.0001$. (G) K-means cluster distribution for the same vectors. $P < 0.0001$ by Chi-squared test. (For interpretation of the references to colour in this figure legend, the reader is referred to the Web version of this article.)

(Sakhi et al., 2014b) habenula display spontaneous neural activity that varies across a circadian cycle. To assess whether this is also the case in the zebrafish habenula, we carried out calcium imaging at ~15 Hz at a single plane. We imaged at two different time points, starting at ZT3 and ZT15, as this was the peak and trough of clock gene expression. The z-score for fluorescence of each cell was calculated, and a vector was generated for the activity of cells with high variance. A difference was observed between the means of this vector at ZT3 and ZT15 (Fig. 3F; $p < 0.0001$ for cytoplasmic label and $p < 0.0001$ for nuclear label; KS test). To further characterize the activity, cells were classified using K-means clustering. The cluster composition was distinct between day and night (Fig. 3G; $p < 0.0001$ Chi-squared test). To test the robustness of this apparent difference, we asked if a classifier could correctly assign a random dataset to either ZT3 or ZT15. Indeed, 21 out of 26 datasets of the cytoplasmic indicator and 10 out of 13 datasets with the nuclear indicator were correctly assigned. These findings suggest that neural activity in zebrafish habenula is different at day versus night.

3.3. *Expression of a truncated clock gene in the habenula affects function*

The expression of clock genes and the circadian change in intracellular calcium in the habenula raises the possibility that an intrinsic clock influences habenula function. To test this, we selectively expressed a truncated *clocka* gene (Dekens and Whitmore, 2008), referred to as Δ*clocka*, in the habenula. This construct has been shown to act in a dominant manner to inhibit the molecular clock in the zebrafish pineal (Livne et al., 2016). Δ*clocka* was expressed in the habenula using the GAL4/UAS system with *TgBAC(gng8:GAL4)* (Hong et al., 2013) as the driver. In addition to *Δclocka*, the effector construct also included enhanced green fluorescent protein (EGFP), which was separated from ΔClocka (ΔCLK) by a 2A peptide linker, thus enabling the expression of two separate proteins. The presence of EGFP in the habenula neurons of *Tg(gng8:GAL4, UAS:EGFP-Δclocka)* fish (Fig. 4A and B) indicates that the construct is expressed appropriately and enables convenient identification of ΔCLK-positive individuals (Livne et al., 2016). Labelling with an antibody against the Myc tag, which is fused in frame at the C-terminus of ΔCLK, indicates that the truncated protein is translated (Fig. 4C). Cells expressing ΔCLK would be expected to have a lower level of Clock-regulated genes such as *per*, than non-expressing cells. To assess this, qHCR imaging was performed on larvae with scattered expression of ΔCLK, and the level of *per3* in cells with EGFP expression was compared with the ratio in non-expressing cells in the same sample. As seen in Fig. 4D the level of *per3* differed between ΔCLK and control cells at all time points, with a paired Cohen's D of 1.58 [95.0%CI 1.03, 4.22; $p = 0.0049$ paired *t*-test] at CT3, 0.525 [95.0%CI 0.337, 4.25; $p = 0.0115$] at CT7, -1.89 [95.0%CI -4.78, −0.734; $p = 0.0554$] at CT11, -1.57 [95.0%CI -3.38, −1.15; $p = 0.0185$] at CT15, 0.872 [95.0%CI 0.636, 2.26; $p = 0.0017$] at CT19 and 0.637 [95.0%CI 0.536, 0.816; $p = 0.0167$] at CT23. This suggests that expression of ΔCLK influences the molecular clock, although it does not eliminate cycling.

Given the partial inhibition shown by gene expression analysis, we asked whether there is any evidence that expression of ΔCLK affects habenula function. The habenula regulates the broad release of serotonin and dopamine (Amo et al., 2010; Satar et al., 2020) and contains

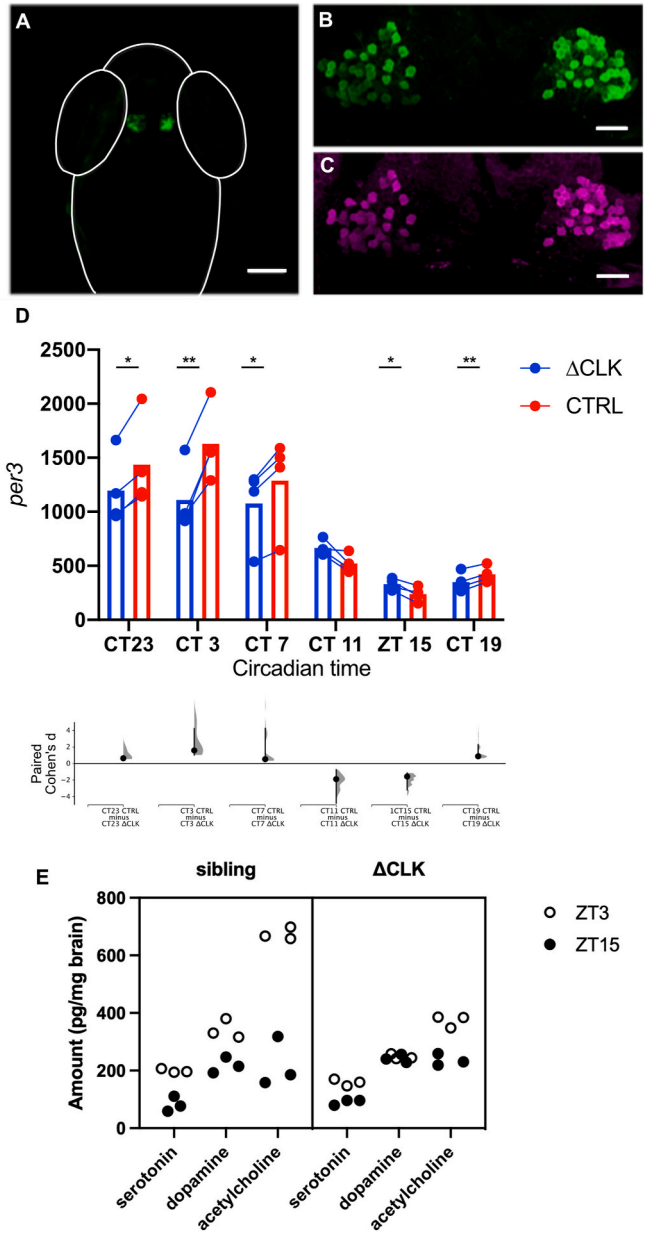

Fig. 4. The effects of expressing truncated *clocka* in the habenula. (**A**) Specific expression of EGFP in the habenula of a *Tg(gng8:GAL4, UAS:EGFP-Δclocka)* fish. (**B**) At higher magnification, EGFP is visible in the cytoplasm of habenula neurons. (**C**) Detection of Myc, which is fused to the C-terminus of ΔCLK, in the habenula of transgenic fish. **(D)** Level of *per3* in the habenula of fish with mosaic expression of EGFP-ΔCLK, as determined by qHCR imaging. The lower graph shows Cohen's d, indicating the degree of difference between ΔCLK-expressing and non-expressing cells at each time point. Values are given in the main text. **(E)** Effects of ΔCLK expression in the habenula on global neuromodulator levels. Plot showing the amount of secreted serotonin, dopamine and acetylcholine in the whole brain of and *Tg(gng8:GAL4, UAS:EGFP-Δclocka)* and sibling fish (N = 3) at ZT3 and ZT15. Fish with ΔCLK expression in the habenula have a reduced day-night change in levels. Scale bar = 100 μm in panel A, 20 μm in panels B and C; * indicates $p < 0.05$; ** indicates $p < 0.005$ by paired *t*-test. Exact p values are provided in the text.

cholinergic neurons (Hong et al., 2013). If expression of ΔCLK has any effect on habenula function, the global levels of secreted serotonin, acetylcholine and dopamine, which vary in a circadian fashion (Hut and Van der Zee, 2011; Mendoza, 2017), should be affected. To test this, brains were isolated from adult zebrafish expressing EGFP-ΔCLK and from their non-expressing siblings, at ZT3 and ZT15. The supernatant from extracts were analysed by liquid chromatography and mass spectrometry (LC/MS) (Chatterjee and Gerlai, 2009). While non-expressing fish had a clear difference in the day- and night-time levels of dopamine (Fig. 4E; mean difference = 124 pg/mg, $p < 0.008$ by Students t-test), there was almost no difference in fish expressing ΔCLK protein (mean difference = 6.3 pg/mg, $p = 0.547$ by Student's *t*-test). The mean difference in between day and night-time levels of serotonin and acetylcholine levels was also higher in control fish (117 pg/mg and 454 pg/mg respectively, $p = 0.002$ and 0.001 by Student's *t*-test), compared to ΔCLK-positive fish (68.1 pg/mg and 137 pg/mg respectively, $p = 0.001$ by Student's *t*-test in both cases). This change of neuromodulator levels is consistent with the notion that expression of ΔCLK in the habenula affects function.

3.4. Habenula expression of ΔCLK reduces anxiety-like behaviour induced by the alarm substance

We hypothesized that a stress response would be affected by the expression of ΔCLK in the habenula. One such response for fish is the alarm response, which is triggered by the pheromone *Schreckstoff*. In adult zebrafish, Schreckstoff causes an acute change in swimming behaviour (Jesuthasan and Mathuru, 2008; Speedie and Gerlai, 2008). Following transient exposure to *Schreckstoff*, fish display abnormal scototaxis (Maximino et al., 2014) and heightened vigilance. To determine whether manipulation of the habenula clock influenced the acute response, adult fish were placed individually in a test tank. After a period of acclimatization, the alarm substance was introduced into the tank (Fig. 5A). Adult *Tg(gng8:GAL4, UAS:EGFP-Δclocka)* zebrafish showed an increase in darting (Fig. 5C, paired mean difference of 1.33 s [95.0% CI 0.5, 2.67], $p = 0.0260$ Wilcoxon rank sum test), as did their non-expressing siblings (paired mean difference of 1.25 s [95.0% CI 0.417, 3.33], $p = 0.0256$ Wilcoxon rank sum test). There was no difference in the movement to the tank base (Fig. 5D; paired mean difference of 16.4 [95.0%CI 1.02, 41.2], $p = 0.530$ for ΔCLK fish and 12.6 [95.0%CI -0.997, 28.1], $p = 0.182$ for siblings).

To monitor expectation of danger (or anxiety-like behaviour), individual fish were exposed to the alarm substance in a beaker, then transferred to a novel tank containing fresh water (Fig. 5E). Control fish showed a reduction in speed (Fig. 5F), which is stronger in the first 2 min after transfer (Fig. 5G; Cohen's d of 1.69 [95%CI 0.81, 2.52], $p = 0.00538$ Mann Whitney). We also monitored the post-exposure response of larval zebrafish, using a light-dark choice assay as an indicator of stress (Steenbergen et al., 2011) (Fig. 5H). Larval *Tg(gng8:GAL4, UAS:EGFP-Δclocka)* fish displayed less dark avoidance after transient exposure to Schreckstoff, as indicated by the increased amount of time spent in the dark side of the tank (Fig. 5I and J; mean difference of 0.0971 [95.0% CI 0.0475, 0.146], $p = 0.001$ permutation *t*-test; Cohen's d = 1.16 [95% CI 0.481, 1.82]), in contrast to their non-expressing siblings (mean difference of 0.0213 [95.0% CI -0.058, 0.0928], $p = 0.588$; Cohen's d = 0.224 [95% CI -0.667, 10.8]). Together, these observations suggest that disruption of the habenula clock leaves acute responses unaffected but reduces the expectation of danger that is evoked by transient exposure to the alarm substance.

We next asked whether the expectation of danger induced by the alarm substance varies in a circadian fashion in zebrafish; a circadian change has been noted in another species, *Rasbora heteromorpha* (Thines and Vandenbussche, 1966). To do this, we exposed larval fish to the alarm substance either at ZT3 or ZT15. Larval zebrafish respond to the alarm substance by extended immobility (Jesuthasan et al., 2020). To sensitively detect this, a vibration was presented 5 min before and after delivery of the alarm substance (Fig. 6A). Control zebrafish showed a reduction in startle after delivery of the alarm substance during the day (ZT3, $p = 0.00248$, Pearson's chi-squared test in R), but not at night (ZT15, Fig. 6B), consistent with freezing during the day but not at night. *Tg(gng8:GAL4, UAS:EGFP-Δclocka)* fish did not show a reduction in startle at day or at night (Fig. 6C). These data suggest that the extended

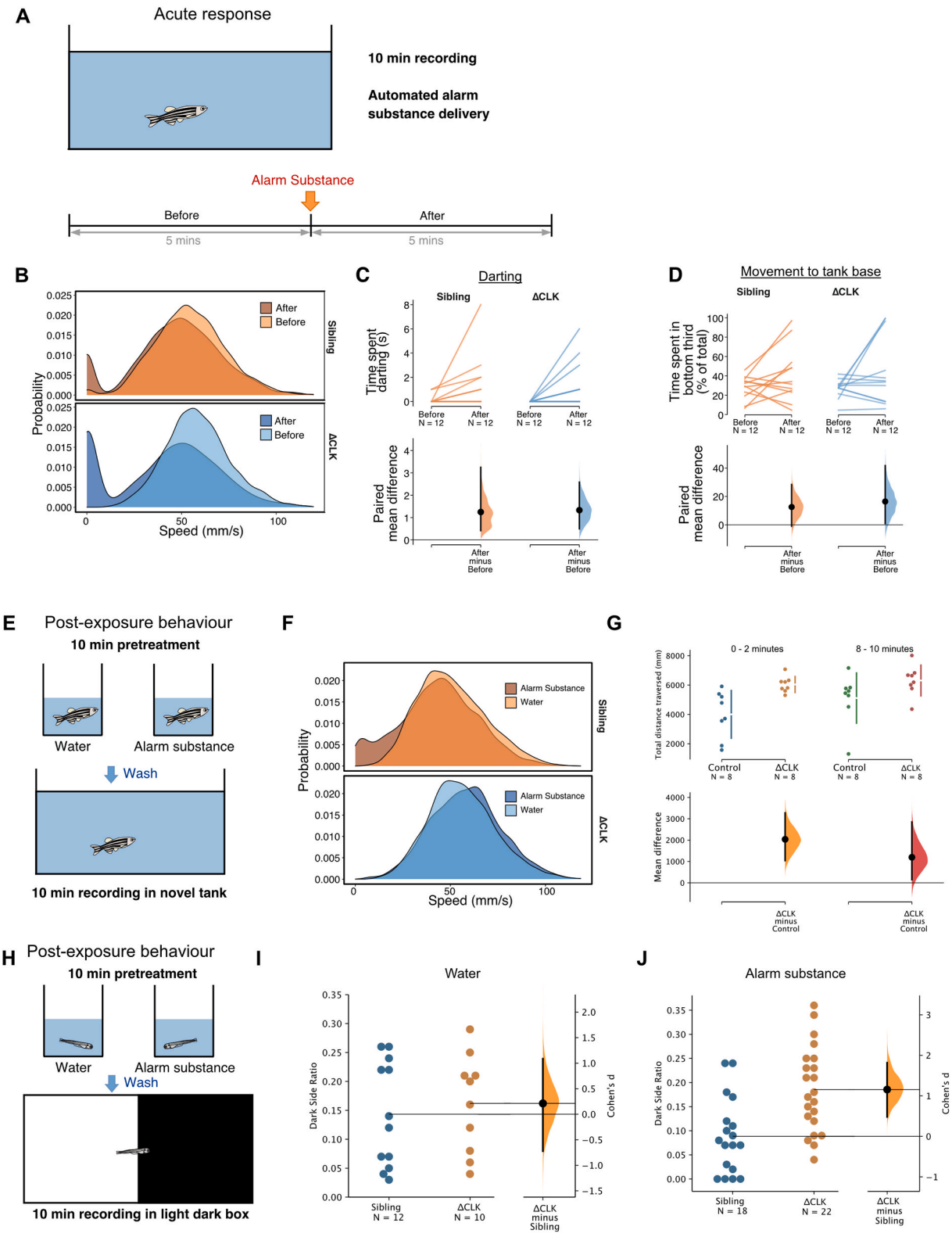

Fig. 5. The effects of the alarm substance *Schreckstoff* on *Tg(gng8:GAL4, UAS:EGFP-Δclocka)* fish. (A–D) Acute effects in adult fish (N = 12). (A) Schematic diagram of the experiment. (B) Speed distribution in fish before and after exposure to the alarm substance, where the substance remained in the tank after delivery. (C–D) Time spent darting (C), restricted to the tank base (D) in the presence of the alarm substance. As indicated by the paired mean difference plots (lower plot), fish with and without expression of truncated *clocka* behave similarly. (E–G) Post-exposure behaviour in adult fish (N = 8). (E) Schematic diagram of the experiment. (F) Speed distribution in a novel tank containing clean water, after exposure to alarm substance or clean water. (G) Distance traversed in a novel tank containing clean water, at different times after exposure to the alarm substance. (H–J) Post-exposure behaviour in 2 week-old zebrafish. (H) Schematic diagram of the experiment. (I) Percentage of time in the dark area of a tank, after 10 min of exposure to embryo water. (J) Percentage of time spent in the dark side after exposure to the alarm substance. *Tg(gng8:GAL4, UAS:EGFP-Δclocka)* fish spend more time in the dark side, with a Cohen's D of 1.2.

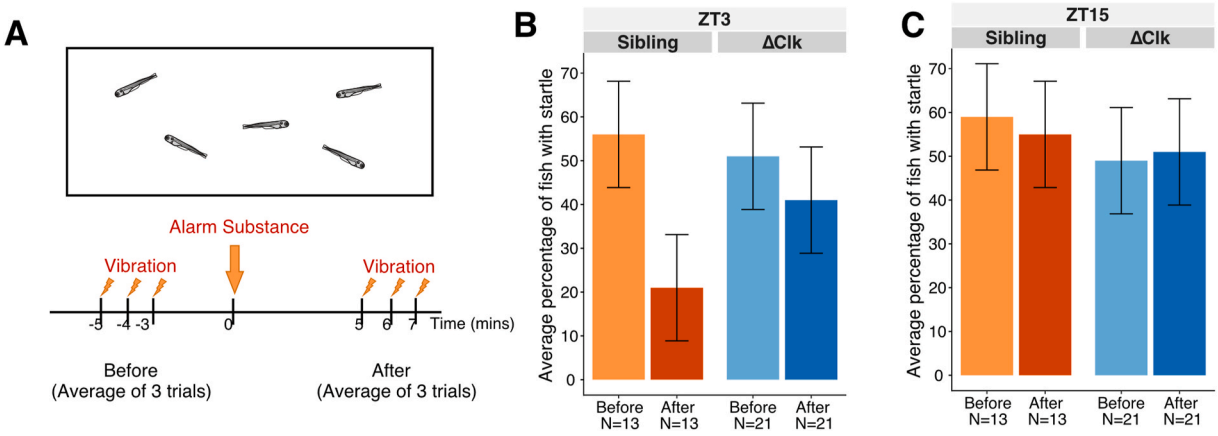

Fig. 6. Day-night variation in the response of zebrafish to *Schreckstoff*. (A) Schematic diagram of the experiment. To assess freezing in larval fish following exposure to the alarm substance, fish were exposed to vibrations in the day (ZT3) (B) or at night (ZT15) (C). Control fish, which are non-expressing siblings of *Tg (gng8:GAL4, UAS:Δclocka)* fish, show a reduction in startle after exposure during the day, but not at night. This response to alarm substance was not seen in *Tg(gng8: GAL4, UAS:Δclocka)* fish in the day or night. Error bars in panels B and C indicate standard deviation.

freezing evoked by the alarm response is circadian in zebrafish and is influenced by the habenula clock.

3.5. Expression of ΔCLK in the habenula does not affect pineal-regulated circadian behaviour

We hypothesized that while the circadian clock in the habenula affects the response to a stimulus that influences expectation, circadian behaviours that are under the control of the pineal clock (Livne et al., 2016) should be unaffected. To test this, we analysed the rhythmic locomotor activity of ΔCLK-positive larvae and their non-expressing siblings. In a normal LD cycle, movement of ΔCLK larvae and siblings were similar (Fig. S2). We next monitored the activity of larvae in constant darkness, to eliminate the masking effects of light and dark on clock-regulated behaviour (Livne et al., 2016). All larvae were entrained to the standard LD cycle before being monitored under constant darkness (DD). As seen in Fig. 7A–E and Table S1, ΔCLK larvae showed a similar pattern of locomotion as their non-expressing siblings, becoming mobile during the light phase and during the subjective day, while exhibiting quiescent periods of inactivity during the 1st and 2nd subjective night of the recording. The amount of activity during the subjective day was similar between ΔCLK and control fish, as judged by the total distance travelled (Fig. S3A; $p = 0.99$ for first subjective day and $p = 0.51$ for second subjective day, by Welch's *t*-test) and amount of rest (Figs. S3B–D; Table S2). During the subjective night, the amount of sleep was similar between ΔCLK and control fish, as measured by sleep bout duration (Fig. 7E; by Welch's *t*-test, $p = 0.54$ by for first night, $p = 0.32$ for second night), frequency of sleep (Fig. 7F; $p = 0.61$ for first night, $p = 0.53$ for second night) and total sleep (Fig. 7G; $p = 0.69$ for first night, $p = 0.24$ for second night).

To further characterize sleep, we examined arousal threshold, which is normally elevated during the sleep-like state at night. Arousal threshold was measured by responsiveness to auditory stimuli (Zhdanova et al., 2001). Nine different intensities were delivered between ZT17 and ZT23, and a sudden change in locomotion was taken as an indicator of responsiveness. A larva was scored as a responder if it moved more than 7 pixels after the stimulus and the average percentage of responders was calculated for each stimulus intensity per group for each experimental run ($N = 5$ experimental runs). Overall, no difference was seen between ΔCLK larvae and their control siblings (Fig. 7H; Table S3).

Finally, we asked whether there was a difference in the movement of ΔCLK fish compared to control fish in the chamber used for the light dark assay during the subjective day, as may occur if there were an effect on sleep. As seen in Fig. S4, the amount of movement was not different (Cohen's $d = 0.59$ [95% CI -0.294, 1.469]; $p = 0.182$ by Student's *t*-test). Together, these results suggest that expressing truncated *clocka* in the habenula does not affect sleep.

4. Discussion

All aspects of life, from arousal state (Scammell et al., 2017) to the ability to handle stress (Daut and Fonken, 2019) and respond to rewards (Antle and Silver, 2015; McClung et al., 2005), vary with time of day. This reflects the tight control exerted by the circadian clock on the physiology and behaviour of animals. Clock genes, which drive the circadian clock, are expressed broadly in the brain (Moore and Whitmore, 2014; Shieh, 2003; Sun et al., 1997). In this paper, we investigated the hypothesis that the habenula clock influences the circadian variation in response to a stressor. We have found that habenula clock in zebrafish is transcriptionally complex, consisting of multiple paralogs. Given the potential redundancy provided by this, we used expression of a truncated *clocka* gene (Dekens and Whitmore, 2008) to manipulate the habenula clock. This strategy is based on the discovery in mice that a truncated *clock* gene disrupts the circadian clock (Vitaterna et al., 1994), whereas a null mutant does not (DeBruyne et al., 2006). Expression of this antimorphic allele in the zebrafish pineal was previously shown to cause a disruption in the expression of clock-regulated genes and in locomotion and sleep (Livne et al., 2016), indicating that it is an effective technique. Expression in the habenula appears to affect the molecular clock, as indicated by the change in *per3* gene expression. We did not observe a complete flattening of *per3* expression across the circadian cycle, however, indicating that inhibition is partial. While consistent with previous findings (Dekens and Whitmore, 2008), this level of inhibition appears sufficient to affect habenula function, as indicated by change in day-night variation in neuromodulators that are under the control of the habenula.

As noted in the methods section, ΔCLK fish were obtained by incrossing to maximize expression in the habenula. The number of non-expressing fish were low. It was noticed that there was a group of fish with a low number of fluorescent cells, and these were also used in the control group. The cut-off is arbitrary but appears functionally significant, however, as seen in the light/dark assay. It is possible that non-expressing cells produce ΔCLK, but the HCR analysis indicates that there is a difference between expressing and non-expressing cells. We have used siblings as controls rather than a different set of wildtype fish, to rule out background differences, which are known to influence behaviour in the zebrafish (Audira et al., 2020; van den Bos et al., 2017;

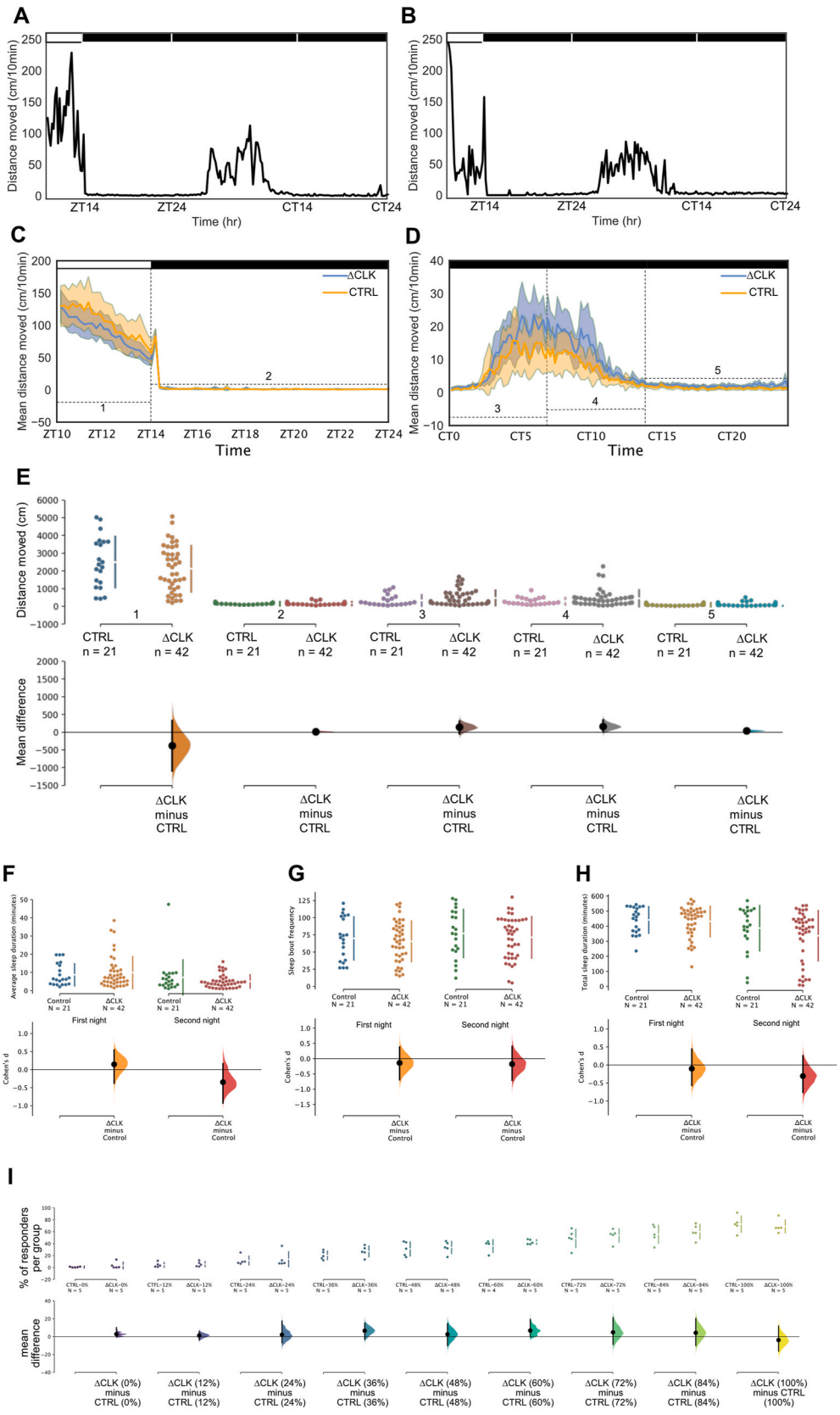

Fig. 7. Sleep is unaltered in *Tg(gng8:GAL4, UAS:EGFP-Δclocka)* larvae

(**A, B**) Distances moved (cm/10 min) by an individual fish from (A) Control group and (B) ΔCLK group, plotted against time (hr) over the time-course of the whole recording. CT = circadian time. (**C, D**) Mean distances moved (cm/10 min) of ΔCLK (blue) and control (orange) groups, plotted against time (hr) (C) during the first 14 h of recording, including 4 h of light-phase and 10 h in the dark during the night (i.e. *Zeitgeber* Time ZT 10–14 and ZT 14–24) and (D) during the subsequent 24 h of recording under DD (i.e. Circadian Time CT 0–24). 95% CIs are indicated by the shaded areas; horizontal brackets indicate 5 timeframes analysed in panel E. Black and white bars represent periods of dark and light, respectively. (**E**) The Cumming estimation plot shows the mean differences in 5 timeframes of the recording: ZT10-14 (1; light-phase), ZT14-24 (2; first night), CT0-7 (3: early subjective day), CT7-14 (4: late subjective day) and CT14-24 (5: subjective night). The upper axis shows the raw data, with each dot representing the overall distance moved (cm) by a single larva; gapped vertical lines to the right of each group indicate mean ± SD. Each mean difference is plotted on the lower axes as a bootstrap sampling distribution. Mean differences are depicted as black dots and 95% CIs are indicated by the end of vertical error bars. (**F–H**) Analysis of sleep during the subjective night. ΔCLK and control fish have similar average sleep bout (F), sleep bout frequency (G) and total sleep (H). (**I**) Analysis of sensory responsiveness of the *Tg(gng8:GAL4, UAS:EGFP-Δclocka)* larvae (7 dpf) during the delivery of auditory stimuli of 9 different intensities. The Cumming estimation plot shows the mean differences for 9 comparisons, corresponding to 9 stimulus intensities (0–100%). The raw data is plotted on the upper axis, each dot representing the percentage of responders per single experimental run. . (For interpretation of the references to colour in this figure legend, the reader is referred to the Web version of this article.)

Manuel et al., 2016). As we do not have the original lines used to generate the Tg (gng8:GAL4, UAS:ΔCLK) fish, a comparison with the relevant wildtype is not possible.

To assess the role of the habenula clock, we used the alarm response in zebrafish as a behaviour paradigm. We observed that the freezing behaviour evoked by the alarm pheromone is lower at night compared to the day, and this difference is reduced by expression of the truncated *clocka* gene specifically in the habenula. We also observed that dark avoidance induced by the alarm substance is reduced by manipulation of the habenula clock. In contrast, the darting and immediate downward movement caused by alarm substance were not affected. No change in circadian behaviours that are unlinked to stressors, such as locomotion or arousal, was observed in fish with ΔCLK expression in the habenula. Together, these observations suggest that the behavioural consequence of disruption of the habenula clock is restricted primarily to anxiety-like behaviour, in contrast to the broader phenotype seen with pineal-specific disruption of the clock (Livne et al., 2016).

One interpretation of these observations is provided by the framework of predictive coding, which has emerged in recent years as a highly effective paradigm for understanding how the brain functions (Clark, 2013; Friston, 2018). A key feature of predictive coding is the updating of expectations based on experience, and this involves the release of neuromodulators that indicate the sign and magnitude of error, as well as precision of prediction. The habenula is one regulator of these modulators, and the pattern of evoked activity and effects of manipulation are consistent with a role in predictive coding underlying motivated behaviour and response to stressors. Recent work has identified a number of mechanisms, such as regulation of membrane potential by astroglial cells (Cui et al., 2018), that influence habenula function by altering the level of spontaneous activity. Spontaneous activity determines the output of a network (Arieli et al., 1996) and is an important element of predictive coding (Hartmann et al., 2015). Here, we propose that the molecular clock, which influences spontaneous activity (Harvey et al., 2020), affects habenula function by altering expectations linked to stressors.

Given the broad expression of clock genes such as *per3* and *cry1a*, it is possible that intrinsic clocks in other components of the network activated by the alarm pheromone e.g. the olfactory bulb, posterior tuberculum or raphe (Jesuthasan et al., 2020), also contribute to circadian variation in the alarm response. Our imaging did not cover this, but work from the Mourrain lab (Leung et al., 2019) indicates that there is circadian variation in neural activity in other regions of the brain. The E-box based clock reporter (Weger et al., 2013) also shows extensive activity. Indeed, there does not appear to be a brain region with no day/night rhythmicity. Nevertheless, the results here establish that disruption of the habenula clock is sufficient to influence the anxiety-like aspect of the response.

Clock gene expression has been reported in the habenula of other vertebrates, including mice (Salaberry et al., 2019). A broad expression of a functional clock in the mammalian habenula is consistent with electrical recordings obtained from slices, which show a change in firing rate and resting membrane potential across the circadian cycle in both medial and lateral habenula (Sakhi et al., 2014a, 2014b; Zhao and Rusak, 2005). The ability of an intrinsic clock to influence habenula-dependent expectations may thus be conserved across vertebrates. This represents a distinct mechanism from the role of clocks in other regions in the regulation of stress (Koch et al., 2017). One implication of the findings here is that identifying clock-regulated genes that regulate spontaneous activity in the habenula may be relevant in the treatment of stress related disorders.

CRediT authorship contribution statement

Adriana Basnakova: Conceptualization, Methodology, Validation, Formal analysis, Investigation, Writing – review & editing, Visualization. **Ruey-Kuang Cheng:** Methodology, Validation, Formal analysis, Investigation, Writing – review & editing. **Joanne Shu Ming Chia:** Methodology, Validation, Formal analysis, Investigation, Writing – review & editing, Visualization. **Giuseppe D'Agostino:** Software, Validation, Formal analysis, Writing – review & editing, Visualization. **Suryadi:** Software, Formal analysis, Visualization. **Germaine Jia Hui Tan:** Investigation, Writing – review & editing. **Sarah R. Langley:** Supervision, Writing – review & editing, Funding acquisition. **Suresh Jesuthasan:** Conceptualization, Methodology, Validation, Formal analysis, Investigation, Resources, Writing – original draft, Visualization, Supervision, Project administration, Funding acquisition.

Declaration of competing interest

The authors declare that they have no known competing financial interests or personal relationships that could have appeared to influence the work reported in this paper.

Data availability

The link to the code is provided in the methods section.

Acknowledgements

We thank Yoav Gothilf for providing the pT2-UAS:EGFP-2A-ΔCLK-5xMYC construct and Marnie Halpern for providing the *TgBAC(gng8:GAL4)*^{c426} line. We also thank Hugh Piggins, David Lyons, Caroline Wee and Ajay Mathuru for comments and discussion, and Erik Meijering for FeatureJ. This work was funded by grants from the Singapore Ministry of Education under its Academic Research Fund Tier 2 (MOE2017-T2-058) and the National Research Foundation (NRF2017-NRF-ISF002-2676) to SJ and an ARAP fellowship from A*Star to AB. SRL was supported by the Lee Kong Chian School of Medicine and Nanyang Technological University Singapore Nanyang Assistant Professor Start-Up Grant, while GDA was supported by the Lee Kong Chian School of Medicine Dean's Postdoctoral Fellowship. The funding agencies played no role in the study design or decision to publish.

Appendix A. Supplementary data

Supplementary data to this article can be found online at https://doi.org/10.1016/j.ynstr.2021.100403.

References

Agetsuma, M., Aizawa, H., Aoki, T., Nakayama, R., Takahoko, M., Goto, M., Sassa, T., Amo, R., Shiraki, T., Kawakami, K., Hosoya, T., Higashijima, S., Okamoto, H., 2010. The habenula is crucial for experience-dependent modification of fear responses in zebrafish. Nat. Neurosci. 13, 1354–1356. https://doi.org/10.1038/nn.2654.

Aibar, Sara, González-Blas, Carmen B., Moerman, T., Huynh-Thu, V.A., Imrichova, H., Hulselmans, G., Rambow, Florian, Aerts, Jan, van den Oord, Joost, Atak, Zeynep Kalender, Wouters, Jasper, Aerts, Stein, 2017. SCENIC: single-cell regulatory network inference and clustering. Nat. Methods 14 (11), 1083–1086. https://doi.org/10.1038/nmeth.4463.

Amezquita, R.A., Lun, A.T.L., Becht, E., Carey, V.J., Carpp, L.N., Geistlinger, L., Marini, F., Rue-Albrecht, K., Risso, D., Soneson, C., Waldron, L., Pagès, H., Smith, M. L., Huber, W., Morgan, M., Gottardo, R., Hicks, S.C., 2020. Orchestrating single-cell analysis with Bioconductor. Nat. Methods 17, 137–145. https://doi.org/10.1038/s41592-019-0654-x.

Amo, R., Aizawa, H., Takahoko, M., Kobayashi, M., Takahashi, R., Aoki, T., Okamoto, H., 2010. Identification of the zebrafish ventral habenula as a homolog of the mammalian lateral habenula. J. Neurosci. 30, 1566–1574. https://doi.org/10.1523/jneurosci.3690-09.2010.

Amo, R., Fredes, F., Kinoshita, M., Aoki, R., Aizawa, H., Agetsuma, M., Aoki, T., Shiraki, T., Kakinuma, H., Matsuda, M., Yamazaki, M., Takahoko, M., Tsuboi, T., Higashijima, S., Miyasaka, N., Koide, T., Yabuki, Y., Yoshihara, Y., Fukai, T., Okamoto, H., 2014. The habenulo-raphe serotonergic circuit encodes an aversive expectation value essential for adaptive active avoidance of danger. Neuron 84, 1034–1048. https://doi.org/10.1016/j.neuron.2014.10.035.

Andalman, A.S., Burns, V.M., Lovett-Barron, M., Broxton, M., Poole, B., Yang, S.J., Grosenick, L., Lerner, T.N., Chen, R., Benster, T., Mourrain, P., Levoy, M., Rajan, K., Deisseroth, K., 2019. Neuronal dynamics regulating brain and behavioral state transitions. Cell 177, 970–985. https://doi.org/10.1016/j.cell.2019.02.037 e20.

Antle, M.C., Silver, R., 2015. Circadian insights into motivated behavior. In: Behavioral Neuroscience of Motivation, pp. 137–169. https://doi.org/10.1007/7854_2015_384.
Arieli, A., Sterkin, A., Grinvald, A., Aertsen, A., 1996. Dynamics of ongoing activity: explanation of the large variability in evoked cortical responses. Science 273, 1868–1871. https://doi.org/10.1126/science.273.5283.1868.
Audira, G., Siregar, P., Strungaru, S.-A., Huang, J.-C., Hsiao, C.-D., 2020. Which zebrafish strains are more suitable to perform behavioral studies? A comprehensive comparison by phenomic approach. Biology 9, 200. https://doi.org/10.3390/biology9080200.
Baño-Otálora, B., Piggins, H.D., 2017. Contributions of the lateral habenula to circadian timekeeping. Pharmacol. Biochem. Behav. 162, 46–54. https://doi.org/10.1016/j.pbb.2017.06.007.
Barrett, L.F., 2017. The theory of constructed emotion: an active inference account of interoception and categorization. Soc. Cognit. Affect Neurosci. 12, 1–23. https://doi.org/10.1093/scan/nsw154.
Berkes, P., Orbán, G., Lengyel, M., Fiser, J., 2011. Spontaneous cortical activity reveals hallmarks of an optimal internal model of the environment. Science 331, 83–87. https://doi.org/10.1126/science.1195870. New York, NY.
Bolte, S., Cordelières, F.P., 2006. A guided tour into subcellular colocalization analysis in light microscopy. J Microsc-oxford 224, 213–232. https://doi.org/10.1111/j.1365-2818.2006.01706.x.
Burgess, H.A., Granato, M., 2007. Modulation of locomotor activity in larval zebrafish during light adaptation. J. Exp. Biol. 210, 2526–2539. https://doi.org/10.1242/jeb.003939.
Cavallari, N., Frigato, E., Vallone, D., Fröhlich, N., Lopez-Olmeda, J.F., Foà, A., Berti, R., Sánchez-Vázquez, F.J., Bertolucci, C., Foulkes, N.S., 2011. A blind circadian clock in cavefish reveals that opsins mediate peripheral clock photoreception. PLoS Biol. 9, e1001142 https://doi.org/10.1371/journal.pbio.1001142.
Chatterjee, D., Gerlai, R., 2009. High precision liquid chromatography analysis of dopaminergic and serotoninergic responses to acute alcohol exposure in zebrafish. Behav. Brain Res. 200, 208–213. https://doi.org/10.1016/j.bbr.2009.01.016.
Cheng, R.-K., Krishnan, S., Jesuthasan, S., 2016. Activation and inhibition of tph2 serotonergic neurons operate in tandem to influence larval zebrafish preference for light over darkness. Sci. Rep.-UK 6, 20788. https://doi.org/10.1038/srep20788.
Chia, J.S.M., Wall, E.S., Wee, C.L., Rowland, T.A.J., Cheng, R.-K., Cheow, K., Guillemin, K., Jesuthasan, S., 2019. Bacteria evoke alarm behaviour in zebrafish. Nat. Commun. 10, 3831. https://doi.org/10.1038/s41467-019-11608-9.
Choi, H.M.T., Schwarzkopf, M., Fornace, M.E., Acharya, A., Artavanis, G., Stegmaier, J., Cunha, A., Pierce, N.A., 2018. Third-generation in situ hybridization chain reaction: multiplexed, quantitative, sensitive, versatile, robust. Development 145, dev165753. https://doi.org/10.1242/dev.165753.
Clark, A., 2013. Whatever next? Predictive brains, situated agents, and the future of cognitive science. Behav. Brain Sci. 36, 181–204. https://doi.org/10.1017/s0140525x12000477.
Csardi, G., Nepusz, T., 2006. The Igraph Software Package for Complex Network Research. InterJournal Complex Systems, p. 1695. https://igraph.org.
Cui, Y., Yang, Y., Ni, Z., Dong, Y., Cai, G., Foncelle, A., Ma, S., Sang, K., Tang, S., Li, Y., Shen, Y., Berry, H., Wu, S., Hu, H., 2018. Astroglial Kir4.1 in the lateral habenula drives neuronal bursts in depression. Nature 554, 323–327. https://doi.org/10.1038/nature25752.
Daut, R.A., Fonken, L.K., 2019. Circadian regulation of depression: a role for serotonin. Front. Neuroendocrinol. 100746. https://doi.org/10.1016/j.yfrne.2019.04.003.
DeBruyne, J.P., Noton, E., Lambert, C.M., Maywood, E.S., Weaver, D.R., Reppert, S.M., 2006. A clock shock: mouse CLOCK is not required for circadian oscillator function. Neuron 50, 465–477. https://doi.org/10.1016/j.neuron.2006.03.041.
Dekens, M.P., Whitmore, D., 2008. Autonomous onset of the circadian clock in the zebrafish embryo. EMBO J. 27, 2757–2765. https://doi.org/10.1038/emboj.2008.183.
Friston, K., 2018. Does predictive coding have a future? Nat. Neurosci. 21, 1019–1021. https://doi.org/10.1038/s41593-018-0200-7.
Germain, Pierre-Luc, Sonrel, Anthony, Robinson, Mark D., 2020. pipeComp, a general framework for the evaluation of computational pipelines, reveals performant single cell RNA-seq preprocessing tools. Genome Biol. 21, 227. https://doi.org/10.1186/s13059-020-02136-7.
Guilding, C., Hughes, A.T.L., Piggins, H.D., 2010. Circadian oscillators in the epithalamus. Neuroscience 169, 1630–1639. https://doi.org/10.1016/j.neuroscience.2010.06.015.
Haghani, S., Karia, M., Cheng, R.-K., Mathuru, A.S., 2019. An automated assay system to study novel tank induced anxiety. Front. Behav. Neurosci. 13, 180. https://doi.org/10.3389/fnbeh.2019.00180.
Haghverdi, L., Lun, A.T.L., Morgan, M.D., Marioni, J.C., 2018. Batch effects in single-cell RNA-sequencing data are corrected by matching mutual nearest neighbors. Nat. Biotechnol. 36, 421–427. https://doi.org/10.1038/nbt.4091.
Hartmann, C., Lazar, A., Nessler, B., Triesch, J., 2015. Where's the noise? Key features of spontaneous activity and neural variability arise through learning in a deterministic network. PLoS Comput. Biol. 11, e1004640 https://doi.org/10.1371/journal.pcbi.1004640.
Harvey, J.R.M., Plante, A.E., Meredith, A.L., 2020. Ion channels controlling circadian rhythms in suprachiasmatic nucleus excitability. Physiol. Rev. 100, 1415–1454. https://doi.org/10.1152/physrev.00027.2019.
Ho, J., Tumkaya, T., Aryal, S., Choi, H., Claridge-Chang, A., 2019. Moving beyond P values: data analysis with estimation graphics. Nat. Methods 16, 565–566. https://doi.org/10.1038/s41592-019-0470-3.
Hong, E., Santhakumar, K., Akitake, C.A., Ahn, S.J., Thisse, C., Thisse, B., Wyart, C., Mangin, J.-M., Halpern, M.E., 2013. Cholinergic left-right asymmetry in the habenulo-interpeduncular pathway. Proc. Natl. Acad. Sci. Unit. States Am. 110, 21171–21176. https://doi.org/10.1073/pnas.1319566110.
Hut, R.A., Van der Zee, E.A., 2011. The cholinergic system, circadian rhythmicity, and time memory. Behav. Brain Res. 221, 466–480. https://doi.org/10.1016/j.bbr.2010.11.039.
Jesuthasan, S., Krishnan, S., Cheng, R.-K., Mathuru, A., 2020. Neural correlates of state transitions elicited by a chemosensory danger cue. Prog. Neuro-psychopharmacol. Biol. Psychiatr. 110110. https://doi.org/10.1016/j.pnpbp.2020.110110.
Jesuthasan, S.J., Mathuru, A.S., 2008. The alarm response in zebrafish: innate fear in a vertebrate genetic model. J. Neurogenet. 22, 211–228. https://doi.org/10.1080/01677060802298475.
Jetti, S.K., Vendrell-Llopis, N., Yaksi, E., 2014. Spontaneous activity governs olfactory representations in spatially organized habenular microcircuits. Curr. Biol.: CB 24, 434–439. https://doi.org/10.1016/j.cub.2014.01.015.
Johnsson, K., Soneson, C., Fontes, M., 2014. Low bias local intrinsic dimension estimation from expected simplex skewness. IEEE T Pattern. Anal. 37, 196–202. https://doi.org/10.1109/tpami.2014.2343220.
Kim, U., Chang, S.-Y., 2005. Dendritic morphology, local circuitry, and intrinsic electrophysiology of neurons in the rat medial and lateral habenular nuclei of the epithalamus. J. Comp. Neurol. 483, 236–250. https://doi.org/10.1002/cne.20410.
Kobayashi, Y., Ishikawa, T., Hirayama, J., Daiyasu, H., Kanai, S., Toh, H., Fukuda, I., Tsujimura, T., Terada, N., Kamei, Y., Yuba, S., Iwai, S., Todo, T., 2000. Molecular analysis of zebrafish photolyase/cryptochrome family: two types of cryptochromes present in zebrafish. Gene Cell. 5, 725–738. https://doi.org/10.1046/j.1365-2443.2000.00364.x.
Koch, C.E., Leinweber, B., Drengberg, B.C., Blaum, C., Oster, H., 2017. Interaction between circadian rhythms and stress. Neurobiol. Stress 6, 57–67. https://doi.org/10.1016/j.ynstr.2016.09.001.
Koren, V., Denève, S., 2017. Computational account of spontaneous activity as a signature of predictive coding. PLoS Comput. Biol. 13, e1005355 https://doi.org/10.1371/journal.pcbi.1005355.
Lee, A., Mathuru, A.S., Teh, C., Kibat, C., Korzh, V., Penney, T.B., Jesuthasan, S., 2010. The habenula prevents helpless behavior in larval zebrafish. Curr. Biol. 20, 2211–2216. https://doi.org/10.1016/j.cub.2010.11.025.
Leung, L.C., Wang, G.X., Madelaine, R., Skariah, G., Kawakami, K., Deisseroth, K., Urban, A.E., Mourrain, P., 2019. Neural signatures of sleep in zebrafish. Nature 571, 198–204. https://doi.org/10.1038/s41586-019-1336-7.
Linson, A., Friston, K., 2019. Reframing PTSD for computational psychiatry with the active inference framework. Cognit. Neuropsychiatry 24, 347–368. https://doi.org/10.1080/13546805.2019.1665994.
Livne, Z.B.-M., Alon, S., Vallone, D., Bayleyen, Y., Tovin, A., Shainer, I., Nisembaum, L. G., Aviram, I., Smadja-Storz, S., Fuentes, M., Falcón, J., Eisenberg, E., Klein, D.C., Burgess, H.A., Foulkes, N.S., Gothilf, Y., 2016. Genetically blocking the zebrafish pineal clock affects circadian behavior. PLoS Genet. 12, e1006445 https://doi.org/10.1371/journal.pgen.1006445.
Lun, A., 2020a. BiocSingular: Singular Value Decomposition for Bioconductor Packages. R package version 1.6.0.
Lun, A., 2020b. Bluster: Clustering Algorithms for Bioconductor.
Lun, A.T.L., McCarthy, D.J., Marioni, J.C., 2016. A step-by-step workflow for low-level analysis of single-cell RNA-seq data with Bioconductor. F1000res. 5, 2122. https://doi.org/10.12688/f1000research.9501.2.
Manuel, R., Gorissen, M., Bos, R. den, 2016. Relevance of test- and subject-related factors on inhibitory avoidance (performance) of zebrafish for psychopharmacology studies. Curr. Psychopharmacol. 5, 1. https://doi.org/10.2174/2211556005666160530122204, 1.
Mathuru, A.S., Kibat, C., Cheong, W.F., Shui, G., Wenk, M.R., Friedrich, R.W., Jesuthasan, S., 2012. Chondroitin fragments are odorants that trigger fear behavior in fish. Curr. Biol. 22, 538–544. https://doi.org/10.1016/j.cub.2012.01.061.
Matias, S., Lottem, E., Dugué, G.P., Mainen, Z.F., 2017. Activity patterns of serotonin neurons underlying cognitive flexibility. Elife 6, e20552. https://doi.org/10.7554/elife.20552.
Matsumoto, M., Hikosaka, O., 2009. Representation of negative motivational value in the primate lateral habenula. Nat. Neurosci. 12, 77–84. https://doi.org/10.1038/nn.2233.
Maximino, C., Lima, M.G., Costa, C.C., Guedes, I.M.L., Herculano, A.M., 2014. Fluoxetine and WAY 100,635 dissociate increases in scototaxis and analgesia induced by conspecific alarm substance in zebrafish (Danio rerio Hamilton 1822). Pharmacol. Biochem. Behav. 124, 425–433. https://doi.org/10.1016/j.pbb.2014.07.003.
McCarthy, D.J., Campbell, K.R., Lun, A.T.L., Wills, Q.F., 2017. Scater: pre-processing, quality control, normalization and visualization of single-cell RNA-seq data in R. Bioinformatics btw777. https://doi.org/10.1093/bioinformatics/btw777.
McClung, C.A., Sidiropoulou, K., Vitaterna, M., Takahashi, J.S., White, F.J., Cooper, D.C., Nestler, E.J., 2005. Regulation of dopaminergic transmission and cocaine reward by the Clock gene. Proc. Natl. Acad. Sci. U. S. A 102, 9377–9381. https://doi.org/10.1073/pnas.0503584102.
McInnes, L., Healy, J., Melville, J., 2018. UMAP: Uniform Manifold Approximation and Projection for Dimension Reduction. Arxiv. https://arxiv.org/abs/1802.03426.
Mendoza, J., 2017. Circadian neurons in the lateral habenula: clocking motivated behaviors. Pharmacol. Biochem. Behav. 162, 55–61. https://doi.org/10.1016/j.pbb.2017.06.013.
Moore, H.A., Whitmore, D., 2014. Circadian rhythmicity and light sensitivity of the zebrafish brain. PloS One 9, e86176. https://doi.org/10.1371/journal.pone.0086176.
Moran, R.J., Campo, P., Symmonds, M., Stephan, K.E., Dolan, R.J., Friston, K.J., 2013. Free energy, precision and learning: the role of cholinergic neuromodulation. J. Neurosci. 33, 8227–8236. https://doi.org/10.1523/jneurosci.4255-12.2013.

Pandey, S., Shekhar, K., Regev, A., Schier, A.F., 2018. Comprehensive identification and spatial mapping of habenular neuronal types using single-cell RNA-seq. Curr. Biol.: CB 28, 1052–1065. https://doi.org/10.1016/j.cub.2018.02.040 e7.

Pennartz, C.M.A., Jeu, M.T.G. de, Bos, N.P.A., Schaap, J., Geurtsen, A.M.S., 2002. Diurnal modulation of pacemaker potentials and calcium current in the mammalian circadian clock. Nature 416, 286–290. https://doi.org/10.1038/nature728.

Pezzulo, G., Zorzi, M., Corbetta, M., 2021. The secret life of predictive brains: what's spontaneous activity for? Trends Cognit. Sci. 25, 730–743. https://doi.org/10.1016/j.tics.2021.05.007.

Ren, J., Qin, C., Hu, F., Tan, J., Qiu, L., Zhao, S., Feng, G., Luo, M., 2011. Habenula "cholinergic" neurons co-release glutamate and acetylcholine and activate postsynaptic neurons via distinct transmission modes. Neuron 69, 445–452. https://doi.org/10.1016/j.neuron.2010.12.038.

Sakhi, K., Belle, M.D.C., Gossan, N., Delagrange, P., Piggins, H.D., 2014a. Daily variation in the electrophysiological activity of mouse medial habenula neurones. J. Physiol. 592, 587–603. https://doi.org/10.1113/jphysiol.2013.263319.

Sakhi, K., Wegner, S., Belle, M.D.C., Howarth, M., Delagrange, P., Brown, T.M., Piggins, H.D., 2014b. Intrinsic and extrinsic cues regulate the daily profile of mouse lateral habenula neuronal activity. J. Physiol. 592, 5025–5045. https://doi.org/10.1113/jphysiol.2014.280065.

Salaberry, N.L., Hamm, H., Felder-Schmittbuhl, M.-P., Mendoza, J., 2019. A suprachiasmatic-independent circadian clock(s) in the habenula is affected by Per gene mutations and housing light conditions in mice. Brain Struct. Funct. 224, 19–31. https://doi.org/10.1007/s00429-018-1756-4.

Satar, N.M.A., Ogawa, S., Parhar, I.S., 2020. Kisspeptin-1 regulates forebrain dopaminergic neurons in the zebrafish. Sci. Rep.-UK 10, 19361. https://doi.org/10.1038/s41598-020-75777-0.

Scammell, T.E., Arrigoni, E., Lipton, J.O., 2017. Neural circuitry of wakefulness and sleep. Neuron 93, 747–765. https://doi.org/10.1016/j.neuron.2017.01.014.

Schindelin, J., Arganda-Carreras, I., Frise, E., Kaynig, V., Longair, M., Pietzsch, T., Preibisch, S., Rueden, C., Saalfeld, S., Schmid, B., Tinevez, J.-Y., White, D.J., Hartenstein, V., Eliceiri, K., Tomancak, P., Cardona, A., 2012. Fiji: an open-source platform for biological-image analysis. Nat. Methods 9, 676–682. https://doi.org/10.1038/nmeth.2019.

Schultz, W., 1998. Predictive reward signal of dopamine neurons. J. Neurophysiol. 80, 1–27. https://doi.org/10.1152/jn.1998.80.1.1.

Scott, E.K., Baier, H., 2009. The cellular architecture of the larval zebrafish tectum, as revealed by Gal4 enhancer trap lines. Front. Neural Circ. 3, 13. https://doi.org/10.3389/neuro.04.013.2009.

Shieh, K.-R., 2003. Distribution of the rhythm-related genes rPERIOD1, rPERIOD2, and rCLOCK, in the rat brain. Neuroscience 118, 831–843. https://doi.org/10.1016/s0306-4522(03)00004-6.

Smith, R., Badcock, P., Friston, K.J., 2021. Recent advances in the application of predictive coding and active inference models within clinical neuroscience. Psychiatr. Clin. Neurosci. 75, 3–13. https://doi.org/10.1111/pcn.13138.

Speedie, N., Gerlai, R., 2008. Alarm substance induced behavioral responses in zebrafish (Danio rerio). Behav. Brain Res. 188, 168–177. https://doi.org/10.1016/j.bbr.2007.10.031.

Steenbergen, P.J., Richardson, M.K., Champagne, D.L., 2011. Patterns of avoidance behaviours in the light/dark preference test in young juvenile zebrafish: a pharmacological study. Behav. Brain Res. 222, 15–25. https://doi.org/10.1016/j.bbr.2011.03.025.

Stringer, C., Pachitariu, M., 2019. Computational processing of neural recordings from calcium imaging data. Curr. Opin. Neurobiol. 55, 22–31. https://doi.org/10.1016/j.conb.2018.11.005.

Sun, Z.S., Albrecht, U., Zhuchenko, O., Bailey, J., Eichele, G., Lee, C.C., 1997. RIGUI, a putative mammalian ortholog of the Drosophila period gene. Cell 90, 1003–1011. https://doi.org/10.1016/s0092-8674(00)80366-9.

Takahashi, J.S., 2017. Transcriptional architecture of the mammalian circadian clock. Nat. Rev. Genet. 18, 164–179. https://doi.org/10.1038/nrg.2016.150.

Tamai, T.K., Young, L.C., Whitmore, D., 2007. Light signaling to the zebrafish circadian clock by Cryptochrome 1a. Proc. Natl. Acad. Sci. Unit. States Am. 104, 14712–14717. https://doi.org/10.1073/pnas.0704588104.

Thines, G., Vandenbussche, E., 1966. The effects of alarm substance on the schooling behaviour of rasbora heteromorpha Duncker in day and night conditions. Anim. Behav. 14, 296–302. https://doi.org/10.1016/s0003-3472(66)80086-6.

Trivedi, V., Choi, H.M.T., Fraser, S.E., Pierce, N.A., 2018. Multidimensional quantitative analysis of mRNA expression within intact vertebrate embryos. Development 145, dev156869. https://doi.org/10.1242/dev.156869.

van den Bos, R., Mes, W., Galligani, P., Heil, A., Zethof, J., Flik, G., Gorissen, M., 2017. Further characterisation of differences between TL and AB zebrafish (Danio rerio): gene expression, physiology and behaviour at day 5 of the larval stage. PloS One 12, e0175420. https://doi.org/10.1371/journal.pone.0175420.

Vitaterna, M., King, D., Chang, A., Kornhauser, J., Lowrey, P., McDonald, J., Dove, W., Pinto, L., Turek, F., Takahashi, J., 1994. Mutagenesis and mapping of a mouse gene, Clock, essential for circadian behavior. Science 264, 719–725. https://doi.org/10.1126/science.8171325.

Wang, H., Yang, Z., Li, X., Huang, D., Yu, S., He, J., Li, Y., Yan, J., 2020. Single-cell in vivo imaging of cellular circadian oscillators in zebrafish. PLoS Biol. 18, e3000435 https://doi.org/10.1371/journal.pbio.3000435.

Weger, M., Weger, B.D., Diotel, N., Rastegar, S., Hirota, T., Kay, S.A., Strähle, U., Dickmeis, T., 2013. Real-time in vivo monitoring of circadian E-box enhancer activity: a robust and sensitive zebrafish reporter line for developmental, chemical and neural biology of the circadian clock. Dev. Biol. 380, 259–273. https://doi.org/10.1016/j.ydbio.2013.04.035.

Wilkinson, S., Dodgson, G., Meares, K., 2017. Predictive processing and the varieties of psychological trauma. Front. Psychol. 8, 1840. https://doi.org/10.3389/fpsyg.2017.01840.

Woods, I.G., Schoppik, D., Shi, V.J., Zimmerman, S., Coleman, H.A., Greenwood, J., Soucy, E.R., Schier, A.F., 2014. Neuropeptidergic signaling partitions arousal behaviors in zebrafish. J. Neurosci. 34, 3142–3160. https://doi.org/10.1523/jneurosci.3529-13.2014.

Yang, Y., Cui, Y., Sang, K., Dong, Y., Ni, Z., Ma, S., Hu, H., 2018. Ketamine blocks bursting in the lateral habenula to rapidly relieve depression. Nature 554, 317–322. https://doi.org/10.1038/nature25509.

Zappia, L., Oshlack, A., 2018. Clustering trees: a visualisation for evaluating clusterings at multiple resolutions. GigaScience 7, giy083. https://doi.org/10.1093/gigascience/giy083.

Zhao, H., Rusak, B., 2005. Circadian firing-rate rhythms and light responses of rat habenular nucleus neurons in vivo and in vitro, 132, pp. 519–528. https://doi.org/10.1016/j.neuroscience.2005.01.012.

Zhdanova, I.V., Wang, S.Y., Leclair, O.U., Danilova, N.P., 2001. Melatonin promotes sleep-like state in zebrafish. Brain Res. 903, 263–268. https://doi.org/10.1016/s0006-8993(01)02444-1.